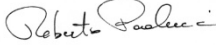




Progress report on 3D physics-based numerical approaches for earthquake ground motion prediction

Work Package#3 "Ground motion"



AUTHORS		REVIEW		APPROVAL	
Name	Date	Name	Date	Name	Date
Paolucci R., Smerzini C., Mazzieri I., Özcebe A.G., Infantino M. 	2018/10/08	J. Douglas 	2018/10/24	 Public-access <input checked="" type="radio"/> SIGMA-2 restricted <input type="radio"/>	2018/10/26

Document history

DATE	VERSION	COMMENTS
2018/07/26	0	
2018/10/08	1	

Executive summary

This document reports the research activities carried out during the first year of the research contract between Politecnico di Milano and swissnuclear “Development of advanced physics-based numerical approaches for earthquake ground motion prediction” (2017-2022), within the SIGMA2 research program.

During the first year of the project, research activities have been addressed to two main tasks: first, the development of novel approaches for ground motion prediction based on physics-based numerical modeling (Task A) and, second, the application of such approaches to the simulation of real case studies (Task B).

Task A has implied a series of studies devoted partly to the numerical implementation of a novel dynamic rupture model in the high-performance Spectral Element Code SPEED and partly to the development of an innovative strategy to generate broadband ground motions starting from the long-period results of physics-based numerical simulations. On the other hand, Task B focused on the simulation of the mainshock of the recent seismic sequence that struck the Norcia area, in Central Italy, in 2016, namely the M_w 6.5 October 30 earthquake. The main outcomes of these activities are summarized below.

A.1) Implementation, testing and validation of a dynamic rupture model

To further enhance the capabilities of the computer code SPEED (see <http://speed.mox.polimi.it/>), part of the research activity of POLIMI has been devoted to the implementation, testing and validation of spontaneous dynamic rupture model. As opposed to kinematic source models, where the spatial and temporal evolution of slip on the causative fault is prescribed, in dynamic source models the initial stress conditions, failure criterion and friction constitutive relationships are prescribed to construct spontaneous fault rupture scenarios.

The dynamic rupture model implemented in SPEED relies on the Coulomb friction conditions between traction and slip and on a linear slip weakening friction to describe the evolution of the friction coefficient with ongoing slip. With respect to the research works already present in literature, the SPEED rupture dynamics algorithm is devised in order to fully exploit the geometrical flexibility and high-order accuracy offered by discontinuous Galerkin methods. In particular, independent non-conforming grids can be used to model the fault geometry and different polynomial approximation degrees can be set into the model to properly approximate the relevant physical quantities involved.

To verify the correct implementation of the dynamic fault rupture in SPEED, the SCEC-TPV3 benchmark was considered. The TPV3 problem consists of simulating a dynamic rupture on a 30 km long by 15 km deep vertical strike-slip fault embedded in a homogeneous elastic full-space. The SPEED solution was compared with the reference synthetics provided by independent codes (ADER-

DG, Spectral Boundary Integral and Finite Difference methods). Results of this verification test indicate, apart from spurious high-frequency oscillations, that SPEED results are in agreement with benchmark solutions, in terms of signal amplitudes, arrival times of the rupture front, stopping phases and subsequent stress relaxation.

A.2) ANN2BB: a novel strategy to produce broadband ground motions from physics-based numerical simulations

To overcome the frequency limitation of physics-based numerical approaches (typically bounded to 1-1.5 Hz), generally not apt to satisfy the needs of engineering applications, a novel strategy has been proposed to generate broadband earthquake ground motions from the results of 3D physics-based numerical simulations. The key idea behind the proposed approach, referred to as ANN2BB, is the use of Artificial Neural Networks (ANN), trained on a set of strong motion records, to predict short period response spectral ordinates from the long-period ones obtained from numerical simulations. The essence of the ANNBB approach is, first, to use the trained ANN to estimate the short period response spectral ordinates using as input the long period ones simulated by SPEED, and, then, to enrich the synthetic time-histories at short periods by scaling iteratively their Fourier spectrum, with no phase change, until their response spectrum matches the ANN target spectrum.

The capability of the proposed approach to reproduce in a realistic way the engineering features of earthquake ground motion, including waveforms in time and frequency domain, peak values and their spatial correlation structure, has been demonstrated for the case study of the M6.0 Po Plain earthquake of May 29, 2012.

B) Applications: the 2016 October 30th earthquake

The mainshock of the 2016 seismic sequence of Central Italy, namely the M_w 6.5 October 30 earthquake in Norcia area, has been considered as main case study to apply, test and validate the numerical tools developed in Task A. The availability of a large set of strong-motion recordings in the epicentral area of the earthquake allowed us to carry out a comprehensive validation study of the results of the 3D physics-based simulations for ground motion prediction in near-source conditions.

During the first year of the project, activities of Task B mainly focused on: i) calibration of the kinematic source model using simpler and faster approaches (Hisada code, based on 3D source but 1D soil model), based on available source inversion solutions; ii) verification of SPEED results with independent codes; iii) construction and calibration of the geological model of the Norcia basin. Preliminary results, reported in this report, indicate that the 3D simulation allows to reproduce with satisfactory accuracy the permanent displacements provided by SAR measurements and the recorded waveforms available at accelerometric stations.

Table of Contents

Document history.....	2
Executive summary.....	2
Introduction.....	5
1. Implementation, testing and validation of fault rupture dynamics in SPEED.....	8
1.1 Overview of the SPEED code	8
1.2 A model of rupture dynamics	10
1.3 Code verification on the SCEC TPV3 problem	11
1.2 Future research activity	12
2. ANN2BB: a novel strategy to produce 3D broadband synthetics from physics-based numerical simulations.....	15
3. Studies on spatial correlation of physics-based synthetics	19
4. 3D numerical simulation of the M_W 6.5 2016 October 30 th Norcia earthquake.....	21
4.1 Set-up of 3D numerical model.....	21
4.2 Overview of 3D numerical simulations	24
4.3 Preliminary results of 3D numerical simulations	25
References	36
APPENDIX 1	39
APPENDIX 2	40
APPENDIX 3	41

Introduction

This report aims at illustrating the main research activities carried out during the first year of the 2017-2022 project “Development of advanced physics-based numerical approaches for earthquake ground motion prediction”, under the cooperation between Politecnico di Milano and swissnuclear, within the SIGMA2 research program.

The project has two main long-term objectives, a first one related to aspects of earthquake ground motion prediction in the context of seismic hazard assessment and a second one covering the issues of the seismic risk assessment of critical facilities, such as Nuclear Power Plants.

These objectives can be summarized as follows:

- Objective 1: development of physics-based hybrid Ground Motion Prediction Equations (GMPEs), based on both synthetics and empirical data, for European regions;
- Objective 2: assessment of fragility curves for exemplarily selected Nuclear Power Plants (NPP) components for the specifically developed near-source ground motion, to evaluate the impact of near-source effects on risk evaluations.

To achieve these two objectives, four main tasks are foreseen, as illustrated in the flowchart of Figure i. In terms of time schedule, the activities related to Objective 1 will be completed in the first three years (2017-2020), while the tasks related to Objective 2 will be carried out in the last phase of the project, from 2020 to 2022.

With reference to the technical organization of SIGMA2 Project, the activity of the POLIMI-swissnuclear collaboration is part of the Work Package 3 “Ground Motion”, Task 3.3.1 - Advanced physics-based numerical approaches for earthquake ground motion prediction. The main goal of WP3 is to improve the prediction of non-ergodic site-specific ground motions through both empirically-based and numerical approaches. Especially in the second phase of the project, synergies with WP6 “Ground Motion for Engineering”, aimed at the improvement of the definition and the use of the seismic motion for industrial studies, will be exploited.

During the first year of the project (May 2017- May 2018), progresses towards two Tasks of the project have been achieved, as described below.

Task A: Advancement in the development of physics-based numerical approaches

Research activities of Politecnico di Milano has been mainly focused on this task and have been devoted towards the following specific objectives:

- (1) implementation, testing and validation of a novel dynamic rupture model in the high-performance Discontinuous Galerkin Spectral Element Code SPEED (for information about the code, see <http://speed.mox.polimi.it/>);
- (2) improvement of approaches for the generation of broadband synthetics starting from the results of 3D physics-based numerical simulations, the accuracy of which is limited to the low frequency range (say up to 1.5-2 Hz). This has been achieved by the development and testing of an innovative technique, that complements classical hybrid methods, based on Artificial Neural Networks trained on strong ground motion recordings to predict short period response spectral ordinates;
- (3) investigation of the issues related to the spatial correlation of earthquake ground motion from 3D broadband physics-based numerical scenarios, to enhance their usability in the framework of seismic risk assessment of large urban areas with spatially distributed portfolios or infrastructural systems.

	Research and Development Program on Seismic Ground Motion	Ref : SIGMA2-2018-D3-015
		Page 6/41

Task B: Applications

With reference to Task B, 3D physics-based numerical simulation of the mainshock of the recent seismic sequence that struck the Norcia area, Central Italy, in 2016, namely the M_w 6.5 October 30 earthquake, has been addressed as a case study to apply the numerical tools developed in Task A. The availability of a large set of strong-motion recordings in the epicentral area of the earthquake allowed us to carry out a comprehensive validation study of 3D physics-based simulations for ground motion prediction in near-source conditions. Efforts were devoted especially to the calibration of the kinematic source model, based on available literature studies, and the collection and processing of geological, geotechnical and geophysical data to construct the numerical model of the Norcia basin. This activity has been partly performed in the framework of the 2017 DPC-RELUIS Project “Numerical simulations of earthquakes and near-source effects”, in collaboration with the University of Pavia.

Results of the numerical simulations shall be considered as preliminary, being still in phase of evaluation and improvement, and will be finalized during the second year of the Project (2018-2019).

The report is organized as follows. In Chapter 1 the main numerical developments of SPEED are described with reference to the implementation of a dynamic source rupture model, in addition to the kinematic model already implemented in the code. In Chapter 2 a novel approach to create realistic 3D physics-based numerical simulations, i.e. the ANN2BB procedure, is presented and applied to a meaningful case study (the M_w 6 2012 May 29 earthquake in the Po Plain, Italy) to test its effectiveness. Chapter 3 focuses on the quantitative analysis of the spatial correlation structure of broadband synthetics by means of geostatistical tools relying on the computation of the semi-variogram of spatially distributed response spectral accelerations at different vibration periods. Finally, in the Chapter 4 the 3D numerical model of the M_w 6.5 2016 Norcia earthquake is presented: the simulated ground motions are analyzed and compared with the available ground motion recordings and broadband shaking maps are produced.

Note that the main text of the chapters contains a brief description of the research work, whereas a more thorough overview of the procedures and of the research achievements is provided in the annexes, attached to this report. For Chapters 2 and 3, the appendices are in the form of papers already published in international journal or conference proceedings.

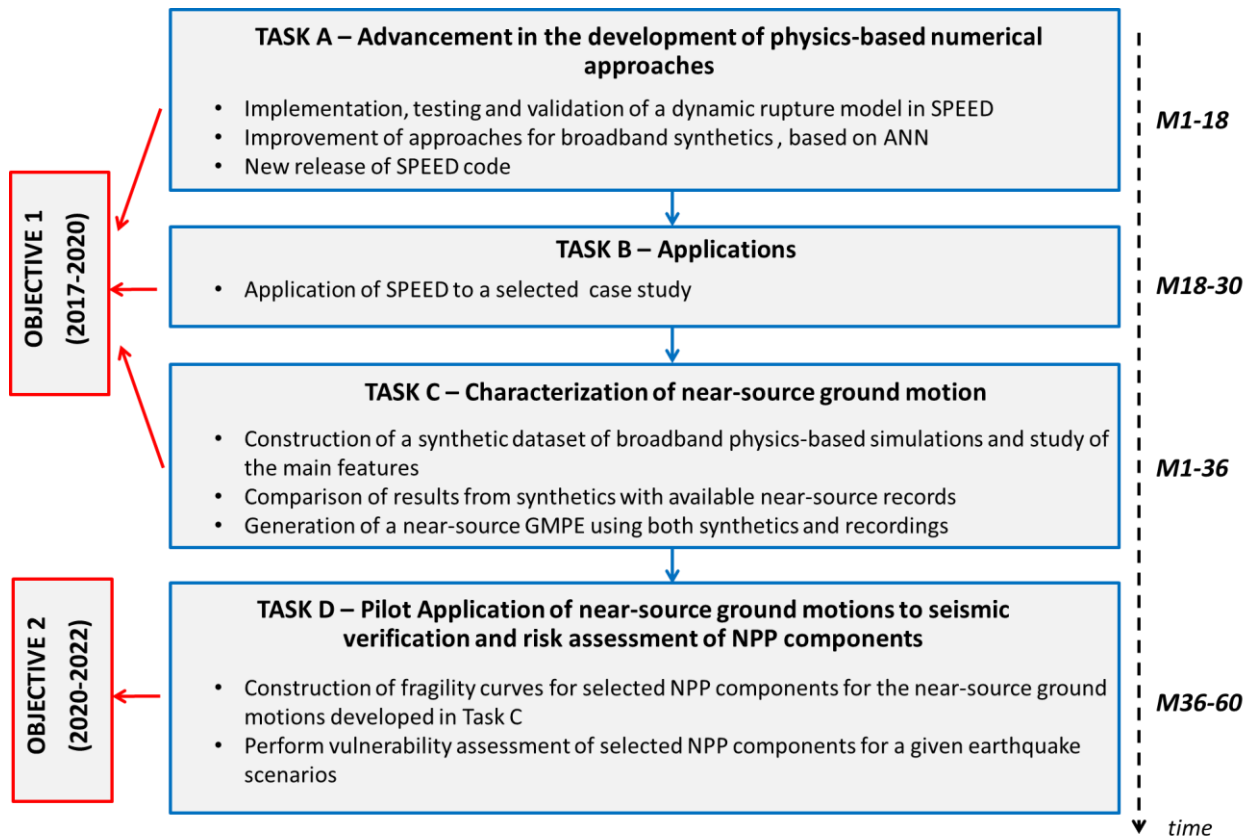


Figure i Project technical overview: main tasks and corresponding time schedule.

1. Implementation, testing and validation of fault rupture dynamics in SPEED

1.1 Overview of the SPEED code

Physics-based numerical modeling of the seismic response of arbitrarily complex earth media has gained major relevance in recent years, owing, on one side, to the ever-increasing progress in computational algorithms and resources, and, on the other side, to the growing interest towards the development of physics based scenarios as input within seismic hazard and risk assessment studies.

Nowadays, 3D numerical models for earthquake rupture dynamics and ground motion simulations are able to include coupled effects of the seismic source, the propagation path through complex geological structures and localized superficial irregularities, such as alluvial basins or/and man-made infrastructures. In the last years, thanks to the ongoing progress of computational algorithms and computing resources, there has been an impressive progress worldwide towards the development of highly accurate numerical methods for the simulation of seismic wave propagation under realistic tectonic and geo-morphological conditions (complex non-planar fault systems, rough surface topography, non-linear rheologies and the heterogeneous structure of the Earth interior).

However, accounting for all these features within a single model still poses challenging demands on computational methods and resources due to the coexistence of very different spatial scales, from a few tens of kilometers, with reference to the seismic fault, up to a few meters, or even less, when considering some structural elements. Motivated by these considerations, a new software SPEED (<http://speed.mox.polimi.it>) was developed, as an open-source high performance numerical code suitable to address the general problem of elastodynamics in arbitrarily complex media (Mazzieri et al. 2013).

SPEED is designed for the simulation of large-scale seismic wave propagation problems including the coupled effects of a seismic fault rupture and the propagation path through complex Earth's layers. Treating numerical problems with such a wide range of spatial dimensions is allowed by a non-conforming mesh strategy implemented through a Discontinuous Galerkin (DG) approach. More specifically, the numerical algorithm can be summarized in the following steps (Figure 1.1): consider an elastic heterogeneous 3D medium, (i) make a partition of the computational domain based on the involved materials and/or structures to be simulated, (ii) select a suitable spectral-element discretization in each non-overlapping sub-region, and (iii) enforce the continuity of the numerical solution at the internal interfaces by treating the jumps of the displacements through a suitable DG algorithm of the interior penalty type (Mazzieri et al. 2013).

By taking advantage of such domain decomposition discretization SPEED allows one to use non-conforming meshes (h -adaptivity) and different polynomial approximation degrees (N -adaptivity) in the numerical model. This makes mesh design more flexible (since grid elements do not have to match across interfaces) and permits to select the best-fitted discretization parameters in each subregion, while controlling the overall accuracy of the approximation. More specifically, the numerical mesh may consist of smaller elements and low-order polynomials where wave speeds are slowest, and of larger elements and high-order polynomial where wave speeds are fastest. Moreover, since the DG approach is applied only at a subdomain level, the complexity of the numerical model and the computational cost can be kept under control, avoiding the proliferation of unknowns, a drawback that is typical of classical DG discretizations.

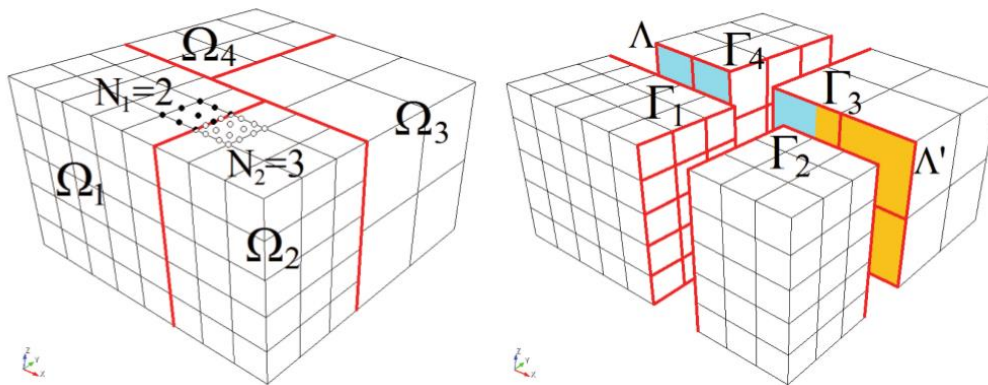


Figure 1.1 3D example of non-conforming domain decomposition. The whole domain is composed by different non-overlapping polygonal subdomains, made by hexahedral elements. Highlighted are the boundary surfaces between different subdomains. DG discretization allows to deal with a non-uniform polynomial degree distribution (N - adaptivity, e.g., $N_1 = 2$ in Ω_1 and $N_2 = 3$ in Ω_2), as well as a locally varying mesh size (h - adaptivity between subdomains Ω_1 , Ω_2 , Ω_3 and Ω_4). The surface between two neighbouring sub-domains Ω_k and Ω_i , then may not be a complete side of Ω_k or Ω_i (e.g. Λ and Λ').

SPEED has been verified over different benchmarks, including that of Grenoble (Chaljub et al. 2010) and the LOH1 test problem (Day et al 2001). Physical discontinuities can be modeled either by the DG approach (creating physical interfaces) or by a not-honoring technique (where material properties are given node by node). The time-integration is performed either by the explicit second-order accurate leap-frog scheme or by the explicit fourth-order accurate Runge-Kutta method. In its present version, SPEED allows the users to treat different seismic excitation modes, including: (i) kinematic seismic fault models (ii) plane wave load; (iii) Neumann surface load; and (iv) volume force load. Dirichlet and/or Neumann boundary conditions can be set into the model. Furthermore, first-order absorbing paraxial boundary conditions (Stacey 1988) have been implemented in order to prevent the propagation of spurious reflections from the external boundaries of the computational domain. Moreover, different attenuation models can be chosen to model visco-elastic soil behavior, specifically: (i) frequency-proportional quality factor Q , as in Kosloff & Kosloff (1986), (ii) frequency constant Q , as in the Generalized Maxwell body model (Emmerich and Korn 1987), and (iii) the classical Rayleigh damping (Chopra 1995). Finally, a non-linear elastic constitutive rheology for the soil is implemented as a generalization to 3D load conditions of the classical modulus reduction and damping curves used within 1D linear-equivalent approaches (see Stupazzini et al. 2009).

To further enhance the capabilities of SPEED, part of the research activity of POLIMI has been devoted to the implementation, testing and validation of spontaneous dynamic rupture model as explained in the following sections and more extensively in Appendix 1.

As opposed to kinematic source models, where the spatial and temporal evolution of slip on the causative fault is prescribed, in dynamic source models the initial stress conditions, failure criterion and friction constitutive relationships are prescribed to construct spontaneous fault rupture scenarios (see Dieterich 1979, Ruina 1983, Mase & Smith 1985). The main advantage of dynamic source modeling is that it can provide insights into the physics driving the fault rupture, including the distribution and magnitude of slip along the fault and its interaction with surrounding conditions, such as stress-changes, free-surface or transient wavefields. As a main drawback, dynamic rupture modeling is much more computationally demanding and it may result in more uncertainties than kinematic source modeling, due to the non-linear nature and initial conditions uncertainties of the underlying physics. Many numerical algorithms have been tested in the past to model dynamic earthquake rupture. Among other, we mention finite differences (FD), boundary integral (BI), finite volume (FV), spectral element (SE) and ADERDG methods (see for instance Dalguer and Day, 2007;

Moczo et al., 2007, Tada and Madariaga, 2001, Benjema et al., 2009, Kaneko et al. 2008, Galvez et al., 2011, Pelties et al. 2012).

With respect to the research works already present in literature, the rupture dynamics algorithm implemented in SPEED is devised in order to fully exploit the geometrical flexibility and high-order accuracy offered by discontinuous Galerkin methods. In particular, independent non-conforming grids can be used to model the fault geometry and different polynomial approximation degrees can be set into the model to properly approximate the relevant physical quantities involved.

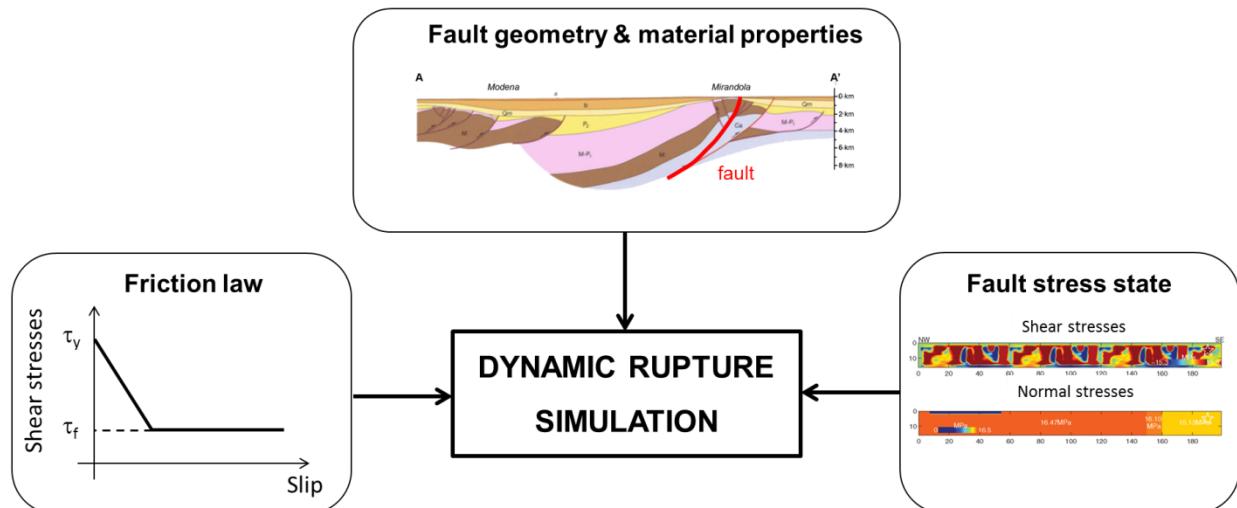


Figure 1.2 Flowchart illustrating the main ingredients of a dynamic rupture model

1.2 A model of rupture dynamics

In the classical three-dimensional dynamic rupture models considered here, a fault is represented by a 2D plane of arbitrary shape (or a set of planes in a segmented fault system) across which fault coplanar displacements can be discontinuous. The kinematics of the sliding process are described by the spatio-temporal distribution of the slip vector $\Delta \mathbf{d} = \mathbf{d}^+ - \mathbf{d}^-$, or the slip rate vector $\Delta \mathbf{v} = d/dt(\Delta \mathbf{d})$, where \mathbf{d}^\pm are the displacements on each side of the fault, in the directions tangential to the fault plane. Even if earthquakes may involve small-scale fault opening, especially at shallow depth, for simplicity, here in the following we consider models in which both sides of the fault remain in contact. On any point of the fault surface, $\sigma_n > 0$ represents the compressive normal stress and $\boldsymbol{\tau}$ the shear traction vector resolved on the + side of the fault. The dynamics of the sliding process are governed by friction relations between traction and slip. The shear traction is bounded by the fault strength $\mu_f \sigma_n$, which is proportional to the normal stress via the friction coefficient μ_f .

Active slip requires the shear traction to reach and remain at the fault strength level, with a direction anti-parallel to the slip rate. These conditions are described by the following equations for Coulomb friction (Andrews 1976):

- (1) $|\boldsymbol{\tau}| \leq \mu_f \sigma_n$,
- (2) $(|\boldsymbol{\tau}| - \mu_f \sigma_n) \leq |\Delta \mathbf{v}| = 0$,
- (3) $\Delta \mathbf{v} |\boldsymbol{\tau}| + |\Delta \mathbf{v}| \boldsymbol{\tau} = 0$.

The evolution of the friction coefficient with ongoing slip is described by the following linear slip weakening friction law:

$$\mu_f = \mu_s - (\mu_s - \mu_d) \min(\delta/D_c, 1),$$

Paolucci et al. –Progress report on 3D physics-based numerical approaches for earthquake ground motion prediction- SIGMA2-2018-D3-015

where μ_s and μ_d are the static and dynamic friction coefficients, respectively, D_c the critical slip distance and δ is the magnitude of the slip, see Figure 1.3. The linear slip weakening friction law is capable of modeling initial rupture, arrest of sliding and reactivation of slip. Due to its simplicity, it is well suited to verify numerical methods with dynamic rupture boundary condition. More advanced realistic friction laws can incorporate rate-and-state effects and thermal phenomena, such as flash heating and pore pressure evolution.

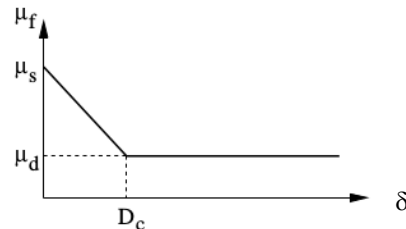


Figure 1.3 Plot of the friction coefficient μ_f as a function of the slip $\Delta\delta$ for the linear slip weakening friction law.

1.3 Code verification on the SCEC TPV3 problem

For geophysically relevant dynamic rupture problems, no analytical solution exists that could be used as a reference for code verification. For this reason the Southern California Earthquake Center (SCEC) created a suite of benchmark problems with increasing complexity for verification of different codes and methodologies.

To verify the correct implementation of the dynamic fault rupture described above in SPEED, we consider one of those problems, namely the TPV3 exercise (Harris et al., 2004). Here, we limit ourselves to illustrate the main results, while the mathematical formulation as well as algorithm details are reported in Appendix 1. *Since it is still an ongoing research activity, we remark that the results presented in the following can be further improved as it will be explained in the next session.*

The TPV3 problem involves rupture on a 30 km long by 15 km deep vertical strike-slip fault embedded in a homogeneous elastic full-space. The fault is governed by linear slip weakening friction and bounded by unbreakable barriers. The initial fault stresses are homogeneous except on a nucleation zone of higher initial shear stress (Figure 1.4). The friction parameters and background stresses can be found in Table 1. The medium has density $\rho = 2670 \text{ kg/m}^3$, P-wave velocity $V_p = 6000 \text{ m/s}$ and S-wave velocity $V_s = 3464 \text{ m/s}$. We use a conservatively large computational domain, a cube of side length 72 km, to avoid spurious reflections from non-perfectly absorbing boundaries.

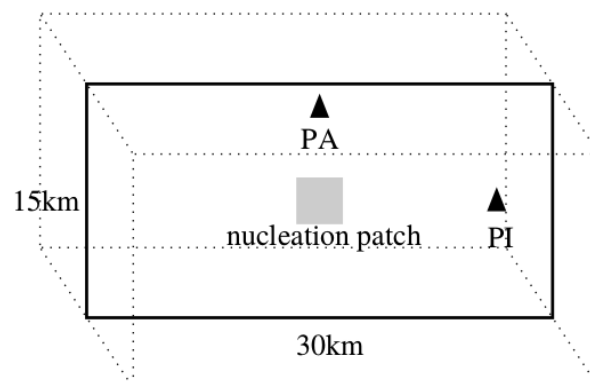


Figure 1.4 Sketch of the SCEC test case with the nucleation zone (grey shaded). The fault is surrounded by a box with an edge length of 72 km. The black triangles indicate the in-plane receiver (PI) and the anti-plane receiver (PA).

Table 1.1 Parameters adopted for the SCEC TPV3 case study.

Parameter	Nucleation zone	Outside nucleation zone
Initial shear traction (MPa)	81.6	70.0
Initial normal stress (MPa)	120.0	120.0
Static friction coefficient	0.677	0.677
Dynamic friction coefficient	0.525	0.525
Critical slip distance (m)	0.4	0.4

We compare the solution obtained by SPEED with the results of the O4 ADER-DG method, of the Spectral Boundary Integral Equation (SBIE) method of Geubelle and Rice (1995) and of a second-order staggered-grid Finite Difference method with traction at split nodes (Day et al., 2005). In particular, we considered three codes that have been verified during the SCEC exercises, the Seissol code (<http://www.seissol.org>), the MDSBI code (<http://pangea.stanford.edu/~edunham/codes/codes.html>) and the Finite Difference code DFM (Dynamic Fault Model). All codes run with a 50 m grid spacing. For the Seissol code this is a sort of equivalent mesh size. Indeed the ADER-DG scheme run on a mesh of increasing size (from 200 m within the fault to 3000 m in the bulk volume) with polynomial order 4 in space and time variables.

In SPEED the fault plane is discretized by a uniform mesh of quadrilaterals with side length $h = 300$ m, and we coarsen the hexahedral elements in the surrounding volume to increase gradually up to 3000 m edge length, to reduce the computational effort. We chose second order polynomial approximation degree and integrate in time with the second order accurate leap-frog scheme, as it is explained in Appendix 1. This leads to an equivalent mesh size of 150 m.

Figure 1.5 shows, for all four schemes, the time histories of the shear stress and slip rate at the two fault locations indicated as PI and PA in Figure 1.4, which probe the in-plane and anti-plane rupture fronts, respectively, at the hypocentral distance 7500 m and 6000 m, respectively.

The SPEED solution is in satisfactory agreement with the ADER-DG solution (black) and with the results produced by MDSBI (blue) and DFM (red). The signal amplitudes, the arrival time of the rupture front and stopping phases and the subsequent stress relaxation are mutually consistent.

However the SPEED solution present spurious high-frequency oscillations in the slip rates. These numerical artifacts can be reduced by increasing the polynomial order or refining the grid. This analysis is still in progress. For completeness we also report in Figure 1.6 snapshots of the computed shear-stresses, slip rate and slip along the fault at some selected time instants.

1.2 Future research activity

The dynamic model has been implemented in parallel environment. Parallel implementation is mandatory in order to achieve small scale resolution needed for rupture dynamic processes, as it is explained in the previous section. As an ongoing research work, the parallel performance of the dynamic fault rupture implementation will be tested on different sets of grids (including non-conforming ones).

Furthermore, the SPEED code equipped with the new dynamic rupture module will be tested on other benchmark problems proposed by the SCEC community as well as realistic earthquake scenario simulations.

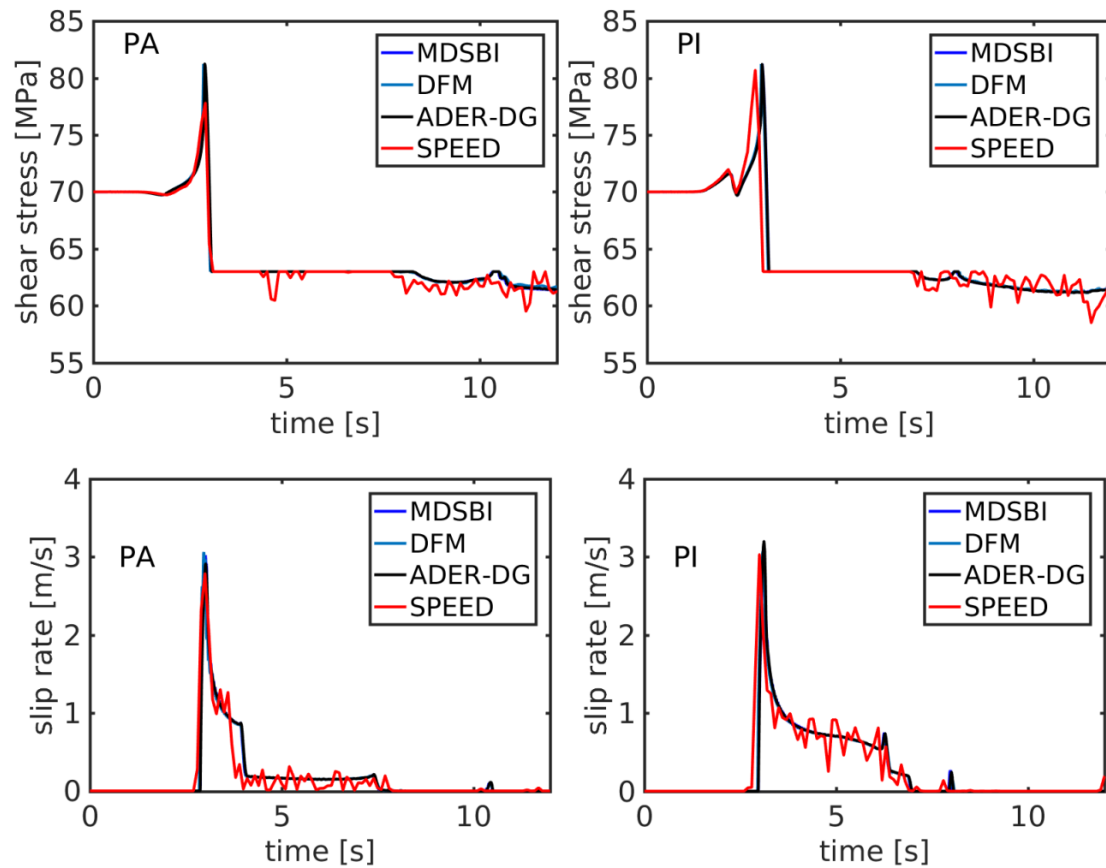


Figure 1.5 Shear stresses (up) and the slip rates (down). PI and PA denote the in-plane and the anti-plane receivers as shown in Figure 1.4.

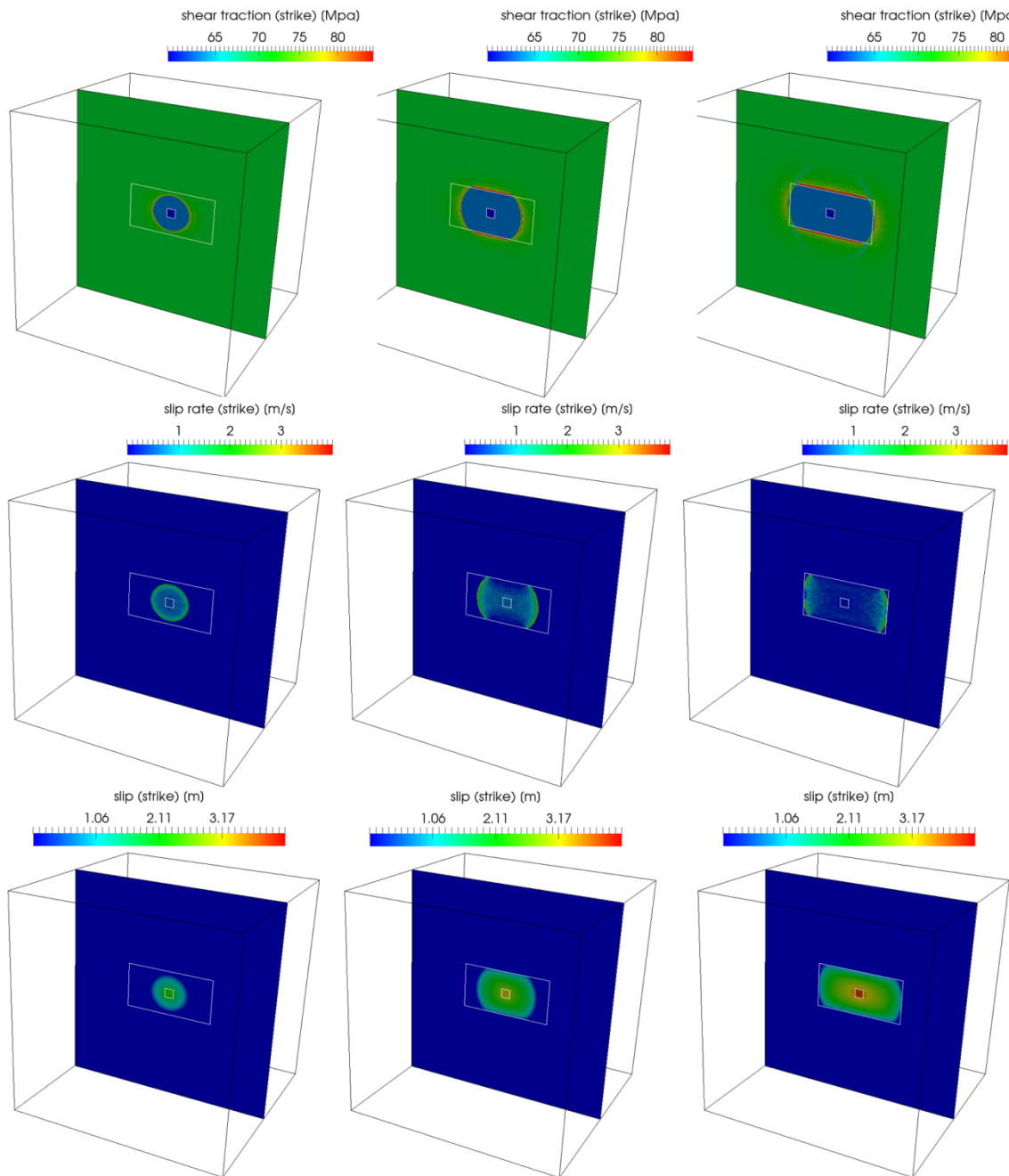


Figure 1.6 Snapshots of the shear stresses (top) the slip rates (center) and slip (bottom) at time $t=3$ s (left), $t=5$ s (middle) and $t=7$ s (right).

2. ANN2BB: a novel strategy to produce 3D broadband synthetics from physics-based numerical simulations

Physics-based numerical simulations (referred to as PBS hereafter) of earthquake ground motion are often advocated as an alternative tool to standard empirical approaches, based on Ground Motion Prediction Equations, since they provide, according to different methodologies, synthetic ground motion time histories compatible with a more or less detailed model of the seismic source process, of the propagation path, and of the local site response. Deterministic approaches rely on the rigorous numerical solution of the seismic wave propagation problem, based on 3D models both of the seismic source (either kinematic or dynamic) and of the source-to-site propagation path. However, the accuracy of the PBS in the high-frequency range is usually bounded up to 1 – 1.5 Hz, owing, on the one hand, to the increased computational burden as the mesh gets finer, and, on the other hand, to the lack of detailed knowledge on the small-scale seismic source features and local geology at short wavelengths. Typically, broad-band (BB) waveforms are produced by a hybrid approach which combines low-frequency results from deterministic PBS with high-frequency signals from stochastic approaches, by gluing the low-frequency and high-frequency portions of the spectrum with amplitude and phase matching algorithms.

To overcome some of the limitations of the hybrid modelling, a novel strategy to generate broadband earthquake ground motions from the results of 3D physics-based numerical simulations (PBSs) is presented. The proposed approach, referred to as ANN2BB hereafter, makes use of Artificial Neural Networks (ANN), trained on a set of strong motion records. The main idea behind this approach is, first, to train an ANN on a strong motion dataset, to correlate short-period ($T < T^*$) spectral ordinates with the long period ones ($T \geq T^*$, being T^* the threshold period beyond which results of the PBS are assumed to be accurate), and, then, use the trained ANN to estimate the short period response spectral ordinates for $T < T^*$, using as input the long period ones obtained by the PBS.

Referring to Appendix 2¹ for a detailed description of the procedure and its application in real case studies, we summarize below the basic steps of the ANN2BB approach. Suppose that an earthquake ground motion scenario is produced based on 3D PBS, which are limited to the long period range $T \geq T^*$. The main steps of the ANN2BB procedure are the following (see Figure 2.1):

- (1) an ANN is trained based on a strong motion records dataset, namely SIMBAD consisting of about 500 records with $M_w=5-7.3$ and epicentral distance up to 35 km (see Smerzini et al. 2014), to predict short period spectral ordinates ($T < T^*$) based on long period ones ($T \geq T^*$). Separate ANNs are trained on the geometric mean of the horizontal components and on the vertical components to allow the prediction of three-component ground motions ;
- (2) for each simulated waveform, a ANN2BB response spectrum is computed, the spectral ordinates of which, for $T \geq T^*$, coincide with the simulated ones, while, for $T < T^*$, they are obtained from the ANN (for both horizontal and vertical components) ;
- (3) the simulated low-frequency waveform is enriched in the high-frequency by a stochastic contribution, characterized by the magnitude and source-to-site distance of the scenario earthquake under consideration;
- (4) the hybrid PBS-stochastic waveform is iteratively modified in the frequency domain, with no phase change, until its response spectrum matches the target ANN2BB spectrum.

¹Appendix 2 reports the paper "Broad-band ground motions from 3D physics-based numerical simulations using Artificial Neural Networks", by R. Paolucci, F. Gatti, M. Infantino, C. Smerzini, A.G. Özcebe and M. Stupazzini, published in the Bulletin of Seismological Society of America, 2018, doi: 10.1785/0120170293

Therefore, the first steps 1-2 allow one to compute, for all PBSs with range of validity $T > T^*$, a site-specific ANN-based broad-band response spectrum, denoted in the following by ANN2BB, as well as maps of peak values of short period ground motion. At this stage, such BB response spectrum does not correspond to a specific waveform. To obtain BB time histories from the ANN2BB spectra, a spectral matching approach is used (step 4), similar to those adopted in the engineering practice to adapt a real accelerograms to a prescribed target spectrum (see NIST, 2011), where the simulated time history is iteratively scaled in the frequency domain, with no phase change, until its response spectrum approaches the target spectrum within a given tolerance. In our case, instead of a recorded accelerogram, we consider the time history resulting from the PBS and, as a target, the ANN2BB spectrum. The difficulty, with respect to the standard spectral matching approach, comes from the low-frequency band-limited nature of the PBS time history, which implies that the high-frequency content of the waveform, essentially consisting of numerical noise, is not usable for scaling. For this reason, before spectral matching to the target ANN2BB spectrum, an intermediate step is done (step 3), where the high-frequency portion of the simulated waveform is enriched by a stochastic component according to the hybrid approach described in Smerzini and Villani (2012).

Further performance tests have been made, on one side, to define the optimal architecture of the ANN in terms of suite of input parameters and, on the other side, to check the performance of the proposed approach with simpler approaches using either a ground motion prediction equation (GMPE) or simple regression-derived equations relating a short-period parameter (e.g. PGA) to a long period one (e.g. SA(1s)). The main findings of these tests are summarized below:

- Preliminary tests on the Po Plain case study (see Figure 2.2) suggest that including magnitude (M_W) and epicentral distance (R_{epi}) as additional input parameters leads to a non-negligible improvement on the results, with a reduction of errors with respect to observations up to about 50%. Further checks are underway to verify the robustness of results; however, a greater improvement is expected in case of training on wider record datasets with larger M_W and R_{epi} ranges;
- Training of specific ANNs on subsets of records, distinguishing between soft and stiff soil conditions, causes a slight decrease of performance with respect to the ANN trained on the complete dataset, because of the decreased number of records considered for each ANN. In future, further tests will be carried out to check the possibility to include V_{S30} as an additional parameter;
- A comparison of the performance of the ANN with simpler approaches based both on data-driven and GMPEs-driven regressions, PGA-SA(3s) and PGA-SA(1s), is shown in Figure 2.3. Results indicate that the ANN reproduces the correlation between short and long period spectral ordinates as found in the training dataset SIMBAD. Although the ANN-driven regressions are compatible with training dataset, they may deviate from the GMPEs regression (especially in terms of PGA-SA3s, left-hand-side graph) because of the specificity of near-source conditions of input dataset. Based on these tests, we expect that the results of ANN are comparable with the ones of a multivariate regression.

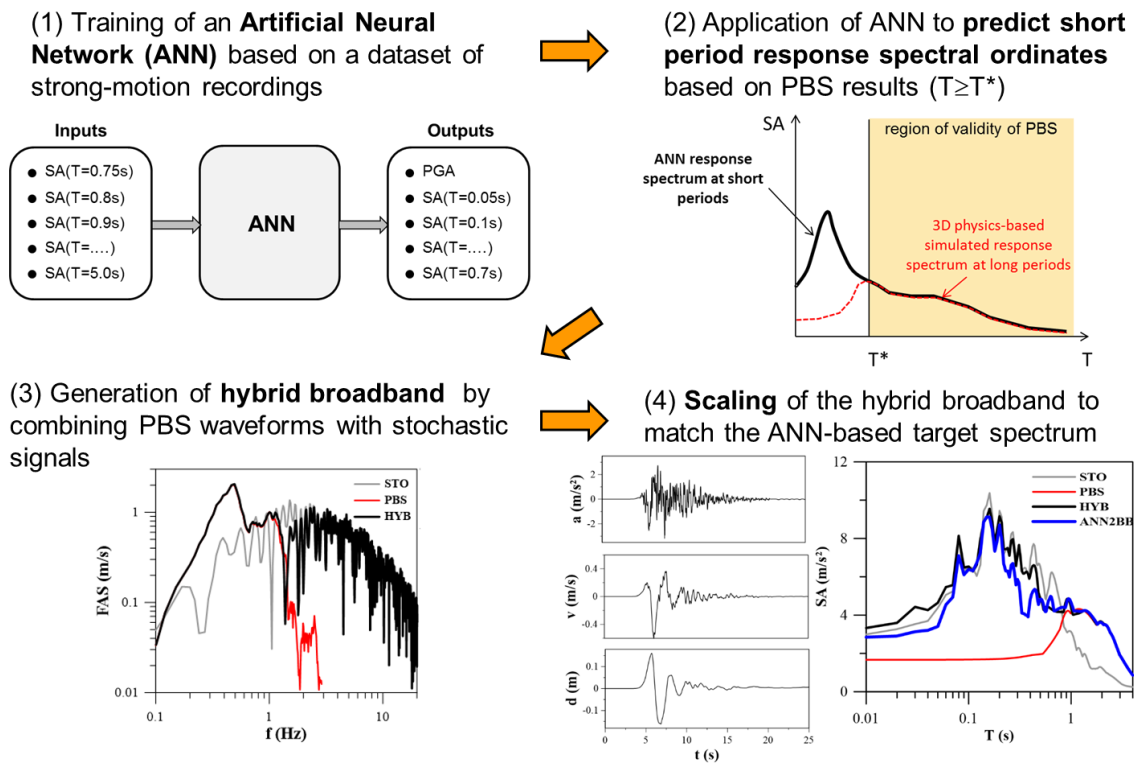
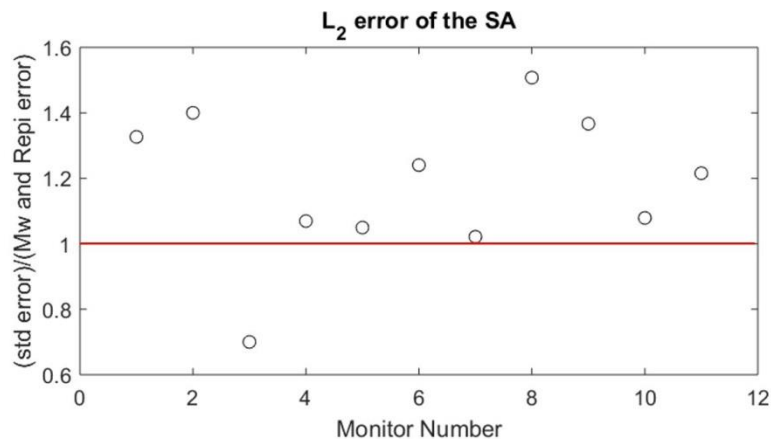


Figure 2.1 Flowchart illustrating the basic steps of the ANN2BB procedure.


 Figure 2.2 Po Plain case study: ratio of L_2 -norm error of the SA (ANN vs Record) obtained for standard ANN (without magnitude M_W and distance R_{epi} as input variable) over that for ANN with M_W and R_{epi} at a set of 11 strong-motion stations. Ratios larger than 1 indicate that including M_W and R_{epi} improves ANN predictions.

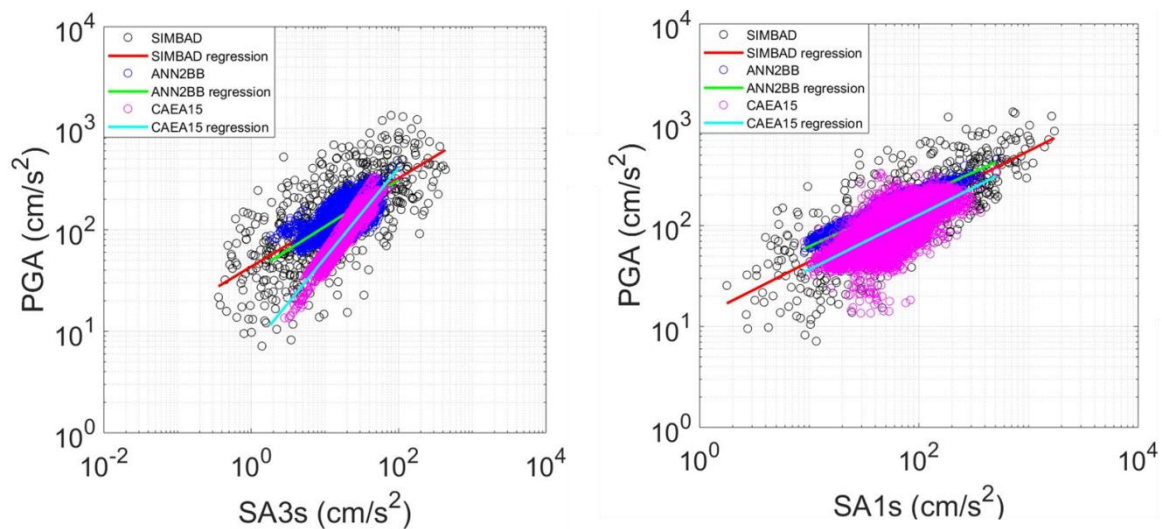


Figure 2.3 PGA-SA(3s) and PGA-Sa(1s) regressions: comparison of SIMBAD data and corresponding linear regression (black symbols and red line) vs ANN2BB predictions and corresponding linear regression (blue symbols and green line) vs GMPE (Cauzzi et al. 2015) predictions and regression (magenta symbols and cyan line).

The ANN2BB approach has been validated against earthquake recordings, particularly for the case study of the May 29, 2012 Po Plain earthquake (Paolucci et al. 2015). Referring to Appendix 2 for a detailed presentation of the results of these validation tests, we report herein the most salient findings:

- similarly to a standard hybrid modeling, the proposed ANN2BB procedure allows one to obtain a realistic aspect of the waveform, both in time and frequency domains ;
- in addition, it also allows one to obtain broadband synthetics which reproduce more closely the correlation features of spectral ordinates of the single waveform, as well as maps of short-period peak values of ground motion featuring a realistic spatial correlation structure of the ground motion itself (see Section 3 for further details).

3. Studies on spatial correlation of physics-based synthetics

Spatial correlation of the ground motion plays a key role in all those applications requiring the definition of the joint occurrence of ground motion intensity measures at several locations during the same earthquake, such as in seismic risk assessment of or spatially distributed portfolios of buildings or infrastructural systems in large urban areas. In this context, GMPEs cannot be used alone, as they cannot account for the spatial correlation structure of ground motion but they should be used in conjunction with suitable empirical spatial correlation models to predict ground motion fields that show the same spatial correlation structures as in real earthquakes (see e.g. Jayaram and Baker 2009; Esposito and Iervolino 2012). On the other hand, physics-based numerical simulations of earthquake ground motion, including a 3D model of the fault rupture, the propagation path and near-surface geology, retains great potential for risk analyses at urban scale, owing to its superiority in reproducing the spatial variability of ground motion at regional scale.

To give further insights into these issues, quantitative analyses of the spatial correlation of broadband physics-based simulated ground motions, generated through the ANN2BB procedure illustrated in the previous Chapter, have been carried out. Geostatistical tools, based on the computation of the semi-variogram and the correlation coefficient as a function of separation distance, have been used to estimate the correlation structure between spatially distributed response spectral accelerations at different vibration periods.

As a comprehensive validation benchmark, the case study of the M6.0 2012 May 29 Po Plain earthquake, with more than 30 near-source recordings available at epicentral distances less than 30 km, has been addressed. As an illustrative example, Figure 3.1 portrays the semi-variograms obtained from records (green), ANN2BB synthetics (red) and hybrid synthetics (blue), for both short period and intermediate periods (PGA and SA at 1.0s on the left and right hand side, respectively). The hybrid synthetics are obtained by combining SPEED waveforms with the stochastic signals from the Sabetta and Pugliese (1996). The horizontal NS component is considered. It is worth noting that PGA has been obtained with ANN2BB procedure (applied for $T < 0.75s$) while SA at 1.0s is the output of 3D PBSs. A good agreement is found between observations and synthetics, with range values of approximately 19-25 km, demonstrating the capability of 3D PBS to reproduce the real correlation structure of ground motion in a broad range of periods. Instead, the hybrid approach produces at short periods (see PGA in Figure 3.1) a semivariogram which is almost flat, thus denoting a zero correlation coefficient at all interstation distances. Note that the low values of the ANN2BB semi-variograms at distances larger than about 40 km may be caused by artificial effects related to the limited number of receiver pairs sampled at separation distance bins which are comparable to the mesh size.

Semi-variogram analyses have been, then, extended to the other case studies, including severe near-source earthquake scenarios ($M=6-7+$) in different areas worldwide (Istanbul, Turkey; Thessaloniki, Greece; Beijing, China), to investigate the influence of physical parameters, such as vibration period, source effects, magnitude and azimuth, on spatial correlation features.

Referring to Appendix 3² for a detailed presentation of the adopted geostatistical tools and results in terms of spatial correlation features for the numerical dataset, we limit ourselves to stress the main conclusions of this work:

²Appendix 3 reports the paper "Analysis of the spatial correlation of earthquake ground motion from physics-based numerical simulations", by M. Infantino, R. Paolucci, and C. Smerzini, published in the proceedings of the Workshop BestPSHANI 2 "Best Practices in Physics-based Fault Rupture Models for Seismic Hazard Assessment of Nuclear Installations: issues and challenges towards full Seismic Risk Analysis", Cadarache-Château, France, 14-16 May 2018.

- the Po Plain application (see Figure 3.1) demonstrates that the 3D PBSs, coupled with ANN2BB, can reproduce accurately the actual spatial correlation structure of ground motion with ranges consistent with recordings both at short and long periods;
- the estimates of ranges, i.e. the inter-station distance beyond which the motions tend to be uncorrelated, from PBSs for the four case studies under consideration (Po Plain; Istanbul; Beijing; Thessaloniki) turn out to be comparable with the related literature studies based on earthquake recordings (Esposito and Iervolino, 2012; Jayaram and Baker, 2009);
- spatial correlation estimates show a marked variability, especially at short periods, suggesting that spatial variability of ground motion is region- and scenario- specific, owing to its strong dependence on local geology and source effects in near conditions. Preliminary analyses of the influence of source and wave propagation effects reveal that: (i) higher ranges, i.e. larger correlation distances of ground shaking, are obtained for the more 'directive' scenarios that produce high levels of ground shaking on a more extended area; (ii) a marked dependence on azimuth is found as a consequence of directionality induced by fault rupture propagation; (iii) the impact of magnitude is relevant especially at long periods (about $T \geq 3s$) with lower ranges for larger magnitude.

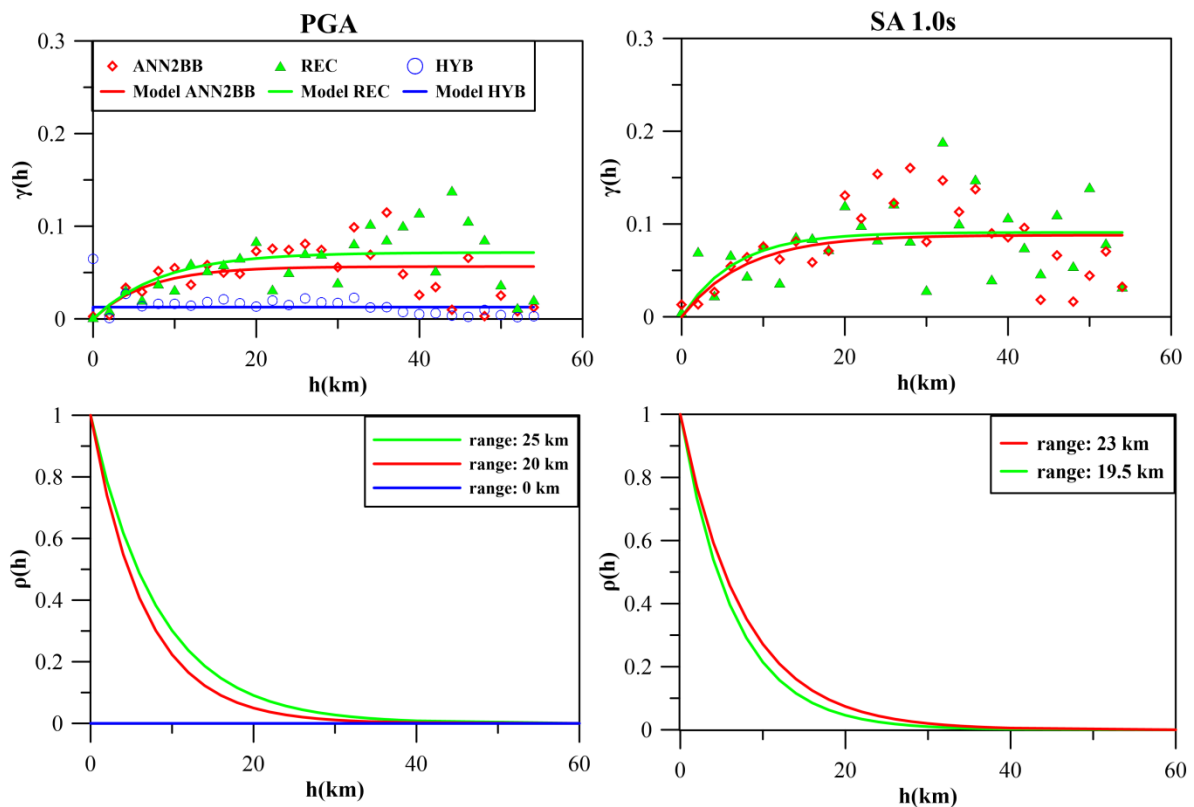


Figure 3.1 M6.0 2012 May 29 Po Plain earthquake: semivariograms (top) and spatial correlation coefficient (bottom) obtained using records REC (triangles, green), the ANN2BB approach (diamonds, red) and the hybrid approach (circles, blue) for PGA (left) and SA(1.0s) (right).

4. 3D numerical simulation of the Mw 6.5 2016 October 30th Norcia earthquake

4.1 Set-up of 3D numerical model

Key ingredients to construct a 3D numerical model for physics-based simulation of a real earthquake are the kinematic source model of the causative fault and the 3D depth velocity model of the region under consideration. Concerning the former, the focus is given in Section 4.1.1 on defining the kinematic model for the M6.5 2016 October 30 Central Italy event with the hypocenter located by the Italian National Institute of Geophysics and Volcanology (INGV) at 42.83° N, 13.11° E at a depth of 9.2 km. For the latter, on the other hand, a careful attempt was carried out to define the 3D geological model for the Norcia basin on which also the city of Norcia, which experienced the strong ground motion at near-fault conditions. Key inputs and methodology followed in the definition of the geological model is synthesized in Section 4.1.2.

4.1.1. Kinematic source model

For the event under consideration, three fault inversion studies are available in scientific literature, namely: CH17 (Chiaraluce et al., 2017), LI17 (Liu et al., 2017), and GA17 (Pizzi et al., 2018). As shown in Figure 4.1, all of the inversions provide fault solutions extending in southeast to northwest with their surface projections covering the epicentral location proposed by INGV.

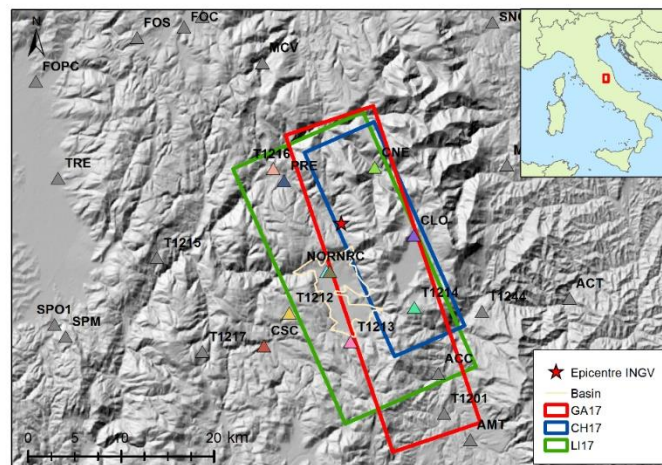


Figure 4.1 Comparison of the surface projections of three available fault solutions (CH17, LI17, and GA17) plotted together with Norcia basin boundaries (yellow), different strong ground motion stations with registrations (triangles), and epicentral location suggested by INGV (red star).

To evaluate the differences between the observations and the simulated ground motion waveforms obtained using each fault solution, preliminary simulations have been performed using the analytical method of Hisada and Bielak (2003). Based on the asymptotic integration of dynamic Green's functions for 3D fault sources in a linear viscoelastic layered half-space, the code allows for a 3D definition of the fault and propagates the seismic waves through a 1D crustal model. In this preliminary phase, Hisada code is used instead of SPEED because it allows one to: 1) verify the results of SPEED by comparison with an independent method (under the same hypothesis of 1D soil model); 2) perform easily a set of parametric analyses to calibrate the finite-fault model to be used as input in SPEED simulations.

In Hisada runs, fault geometry-related properties (strike, dip, rake, and depth of fault) are directly adopted from the relevant publications. Instead, homogeneous definitions of epicentral location, rise time (τ), and rupture velocity (V_{rup}) are provided for all three cases as INGV epicentral coordinates, 0.7 s, and 1700 m/s, respectively. In all of the cases, the crustal structure proposed by Evangelista et al. (2017) is adopted, given that the results are proven not to change when one considered a more detailed definition provided by Hermann et al. (2011).

The analyses of the simulations at several stations showed that the fault solution by GA17 provides a better fit with the observations, especially considering the displacement response. This fault solution has therefore selected for the 3D numerical simulations. In Figure 4.2, the comparison of displacement time histories between observations and simulations (using GA17) at selected five near-fault stations are shown. It is worth noting that, although most of the time histories show a good match, there are a few stations (see NRC-NS, NOR-NS and CNE-EW) where the polarities of the simulations and observations are opposite. Excluding issues in the polarities of recordings (as also confirmed by comparison of recordings with GPS and SAR measurements), such discrepancies are caused by the assumed finite-fault model, which cannot catch the observed wavefield with adequate accuracy at all stations. As a matter of fact, the same issues are found in the synthetics computed using independent codes (Galovic, Pers. Comm. 2018).

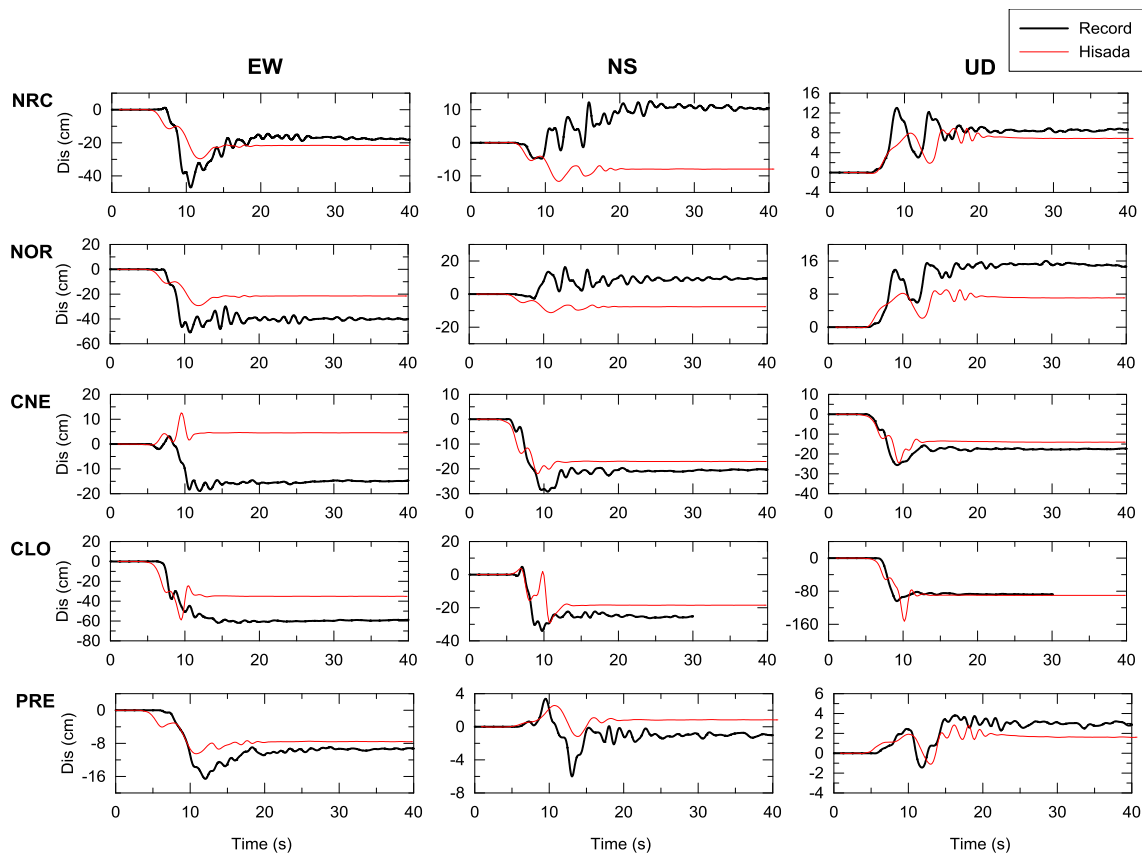


Figure 4.2 Comparison between observations (black) and simulations (red) in terms of displacement time histories using the fault solution of GA17 at five accelerometric stations (the location of the stations is shown in Figure 4.2).

In addition to the assessment of epistemic uncertainty associated with the fault inversion studies, using GA17, an additional sensitivity study was also carried out to evaluate the dependency of results with respect to the model parameters of τ (0.5s, 0.7s, 1.0s) and V_{rup} (1700 m/s, 1955 m/s, 2200 m/s, 2800 m/s). It was found that rise time has negligible effect on the displacement response and affects mainly higher frequencies in the velocity response (specifically, frequencies higher than $1/\tau$). For the

latter, on the other hand, super shear effects leading to large peaks in the velocity responses were observed for all of the cases with $V_{rup} > V_{S,layer1}=1700$ m/s.

In summary, GA17 fault model parameters selected for the 3D physics-based simulations are: *strike angle* = 160°, *dip angle* = 40°, *rake angle* = -90°, $V_{rup} = 1700$ m/s, $\tau = 0.7$ s, *epicentral position* = 42.83° N, 13.11° E, *hypocentral depth* = 9.5 km, *fault length* = 36 km, *fault width* = 13 km, *depth to top of the fault* = 1.8 km.

4.1.2. 3D depth-velocity model of Norcia Basin

In order to construct the depth-velocity model of Norcia basin, extensive effort was spent on collecting data from the scientific and technical literature and local experts³. Current information dataset includes:

- 9 sections: 2 geologic sections obtained from Motti (2017); 2 seismic-reflection sections from Böhm et al. (2011); 5 gravimetric sections from Aringoli et al. (2014);
- 83 H/V tests carried out at various locations: 48 from Angeletti et al. (2018); 20 from Porreca and Vasallo (2018); 15 from Bindi et al. (2011);
- 42 V_S -profiles: 39 from Angeletti et al. (2018); 2 from INGV-Milano; 1 from Bindi et al. (2011);
- 3 V_P -profiles: 2 from Angeletti et al. (2018); 1 from Bindi et al. (2011);
- 3 boreholes associated with SPT measurements (all from Angeletti et al., 2018);
- 4 boreholes associated with geotechnical laboratory tests (all from Venanti et al., 2018).

Spatial distribution of the collected and combined data prior to model generation is shown in Figure 4.3.

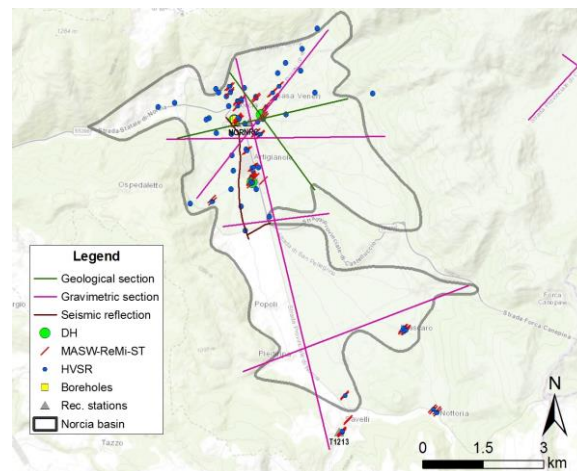


Figure 4.3 Spatial distribution of the combined dataset of collected geophysical and geological information prior to model generation.

While generating the 3D depth-velocity model of the Norcia basin, a 6-step procedure is followed as briefly explained in the following bullet points:

- Idealization of the V_S -profile to be used within the basin as in Figure 4.4;
- Through the equation below, finding out the sediment thickness proxies (H) at the H/V points by using their recorded fundamental frequency (f_0) information and idealized V_S -profile ($V_S(z)$);

$$\int_0^H \frac{dz}{V_S(z)} = \frac{1}{4f_0}$$

³ The work of site characterization was carried out in cooperation with the University of Pavia in the framework of the RS2 Project, within the 2017 DPC-Reluis research programme.

- Digitizing the 9 sediment thickness profiles;
- Combining the sediment thickness proxies with the depth profiles;
- Defining 3D-sediment thickness model through a spatial interpolation scheme implemented in MATLAB (*griddata*) and smoothing the interpolated surface to remove the singularities;
- Combining the sediment thickness model with the topography of the region (i.e. digital elevation model, DEM) to compute the basin surface and top of bedrock elevations.

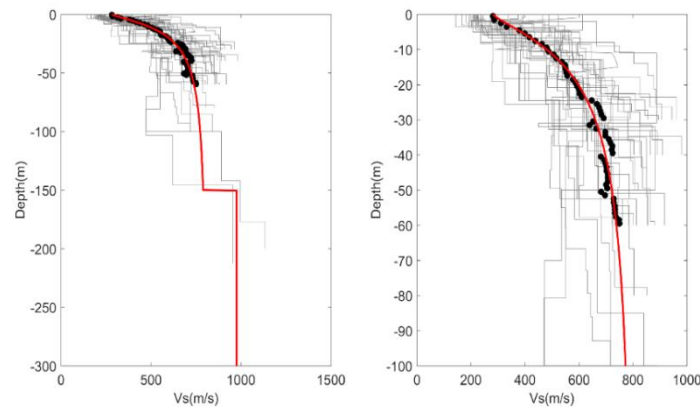


Figure 4.4 Measured (individual measurements: gray lines, averages: black points) and modelled (red line) V_S -depth relation. Left: for a depth range from -300 to 0 m, right: for a depth range from -100 to 0 m. Until -150 meters, depth dependent VS has a functional form with $V_{S,ref}=548.33$ m/s, $V_{S,min}=281.65$ m/s, $z_{ref}=15.0$ m, and $n=1.29$; below -150 meters a constant 975 m/s layer is introduced until the lithologic bedrock level (unknown).

The 3D sediment depth model obtained at the end of Step 6 is provided in Figure 4.5.

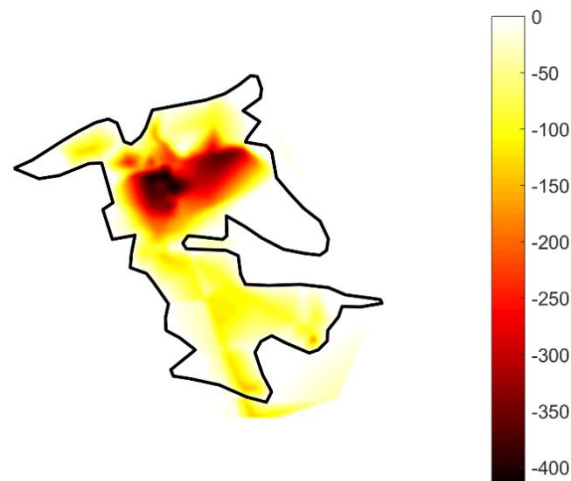


Figure 4.5 Sediment depth model of Norcia Basin. 0: no sediment, -x: depth of bedrock is x meters below the ground surface.

4.2 Overview of 3D numerical simulations

Four different 3D spectral element models are created and analyzed with SPEED code, as listed below and shown in Figure 4.6:

- **Model S-1** (Figure 4.6, 1st from left): 1D topography with the Earth's bedrock layers deposited in parallel according to Evangelista et al. (2017). Basin is not modelled. Model dimensions are 40 km x 50 km x 21 km with nearly 175,000 4th order spectral elements, resulting in maximum usable frequency of 2.0 Hz. Source geometry and its slip distribution are defined according to GA17 model discussed in Section 4.1. Absorbent paraxial boundaries are used all around the external faces.
- **Model S-2** (Figure 4.6, 2nd from left): same as in Model S-1, but with 3D topography. Total number of elements nearly 350,000 with spectral order of 3. Maximum resolvable frequency is around 1.5 Hz.
- **Model S-3** (Figure 4.6, 3rd from left): same as in Model S-2, but with the basin.
- **Model S-4** (Figure 4.6, 3rd from left): same as in Model S-3, but with complex kinematic source, where the rise time is randomized around the mean value of 0.7s according to the procedure presented in Smerzini and Villani (2012).

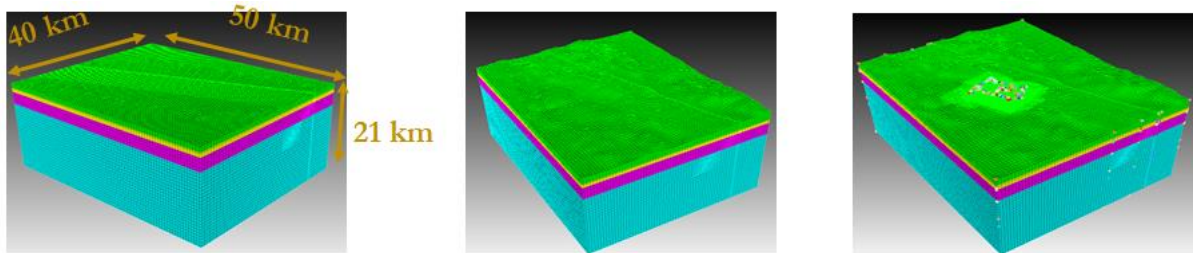


Figure 4.6 Left: Model S-1; Center: Model S-2; Right: Model S-3 and Model S-4.

Source related properties and spatial distributions of slip (S), rupture time (t_0), and rise time (τ) are shown in Figure 4.7. Complex and simple source share the same S and t_0 definitions, thus their difference lies only on τ .

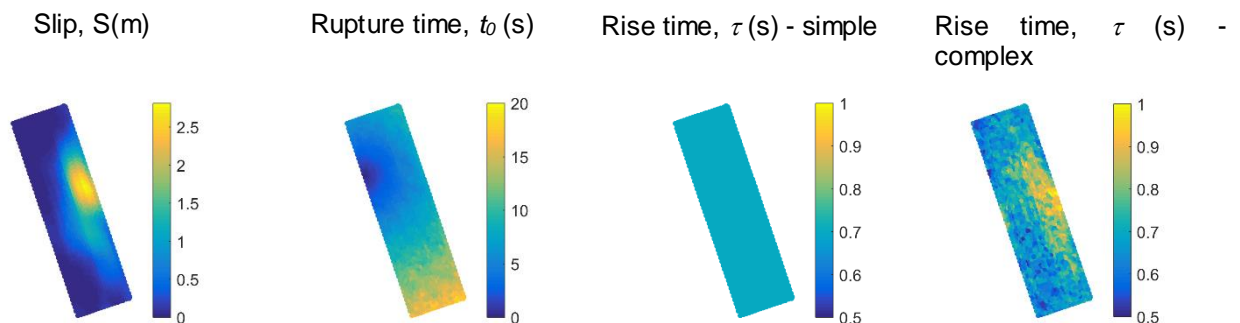


Figure 4.7 Source parameters used in SPEED analyses (left to right: S-1 to S-4). Simple source is used in S-1, S-2, and S-3; Complex source is used in S-4

4.3 Preliminary results of 3D numerical simulations

The preliminary results of the 3D physics-based simulations are presented by the following order:

- Section 4.3.1: Validation of Model S-1 with the results of the final Hisada analysis;
- Section 4.3.2: Comparison of computed velocity time histories using Model S-3 and improvement of results when a more complex source is used;
- Section 4.3.3: Peak ground velocity (PGV) maps created by using Model S-4;
- Section 4.3.4: Presentation of the computed permanent ground displacement map with respect to independent measurements with SAR.
- Section 4.3.5: computation of broadband synthetics from Model S-4 using the procedure illustrated in Chapter 2.

4.3.1. Verification of SPEED model S-1

In Figure 4.8, displacement waveforms along East-West (EW), North-South (NS), and Up-Down (UD) directions computed for the model S-1 are compared with those obtained through benchmark Hisada analyses for five representative stations: NRC, NOR, CLO, CNE, and PRE. It is observed that a satisfactory agreement is reached between two codes, Hisada and SPEED, in the frequency range up to 1 Hz.

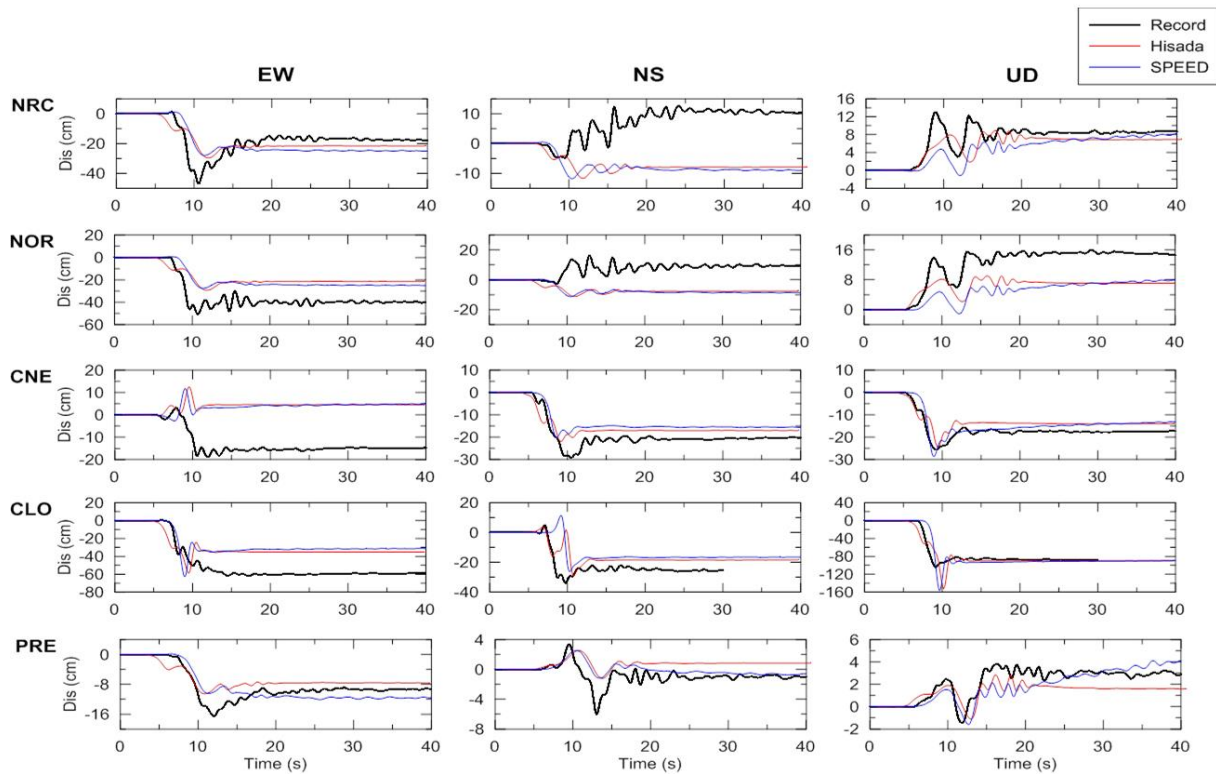


Figure 4.8 Comparison of the displacement waveforms computed through Hisada and SPEED S-1 models and their agreement with recordings for the ITACA stations: NRC, NOR, CNE, CLO, and PRE. All of the waveforms are low-pass filtered at 1 Hz.

4.3.2. Comparison with strong-motion recordings

This section addresses the comparison between recorded and simulated ground motions, the latter being obtained using both the simple source model and an enhanced model obtained after the introduction of source complexity (random rise time).

In Figure 4.9, the comparisons of velocity waveforms computed with Model S-3 with respect to recordings for the stations: NRC, NOR, CNE, CLO, and PRE. Disagreement in the frequency content for relatively small frequencies (~ 1 Hz) is obvious and verified also in terms of Fourier spectra not shown herein for sake of brevity.

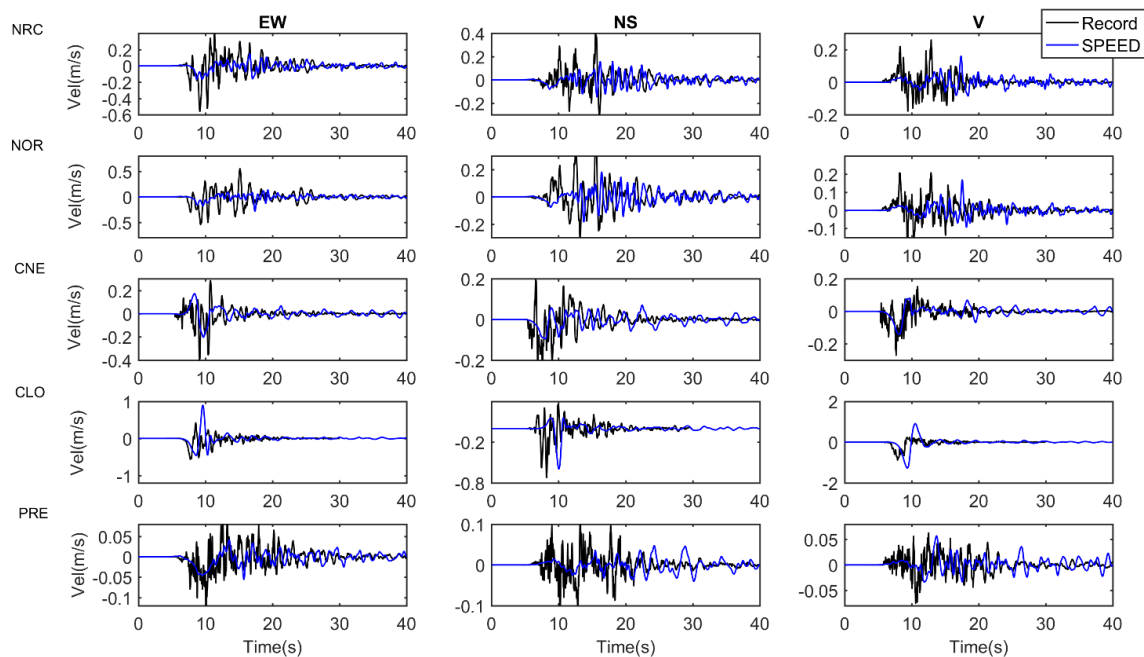


Figure 4.9. Comparisons of velocity time histories of unfiltered recordings (black) and SPEED S-3 simulation results (blue) for the stations: NRC, NOR, CNE, CLO, and PRE.

As the missing frequency content is well inside the frequency range that can be modelled through the numerical simulation (i.e. < 1.5 Hz), source complexity through rise time randomization was introduced to boost the frequency band. In fact, results showed significant improvement in terms of frequency content in the range of 0.8 - 1.5 Hz, as shown in Figure 4.10 for NRC station in both time and frequency domain. To assess quantitatively the misfit between synthetics and recordings, we computed the goodness-of-fit (GoF) scores proposed by Anderson (2004) for NRC station, model S-4. The results, reported in Figure 4.11, indicate that, for most parameters under consideration and on the three components of motion, the fit is good to excellent.

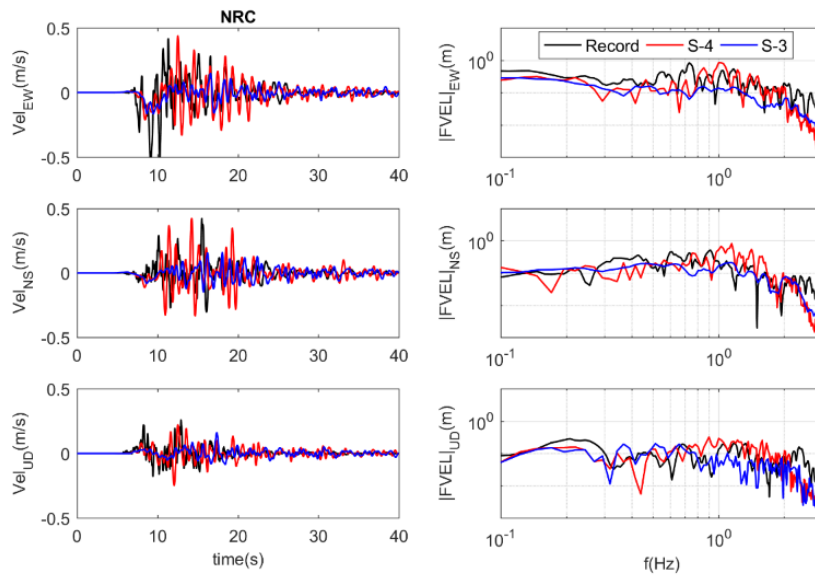


Figure 4.10. Effect of source complexity in terms of velocity response of NRC station.

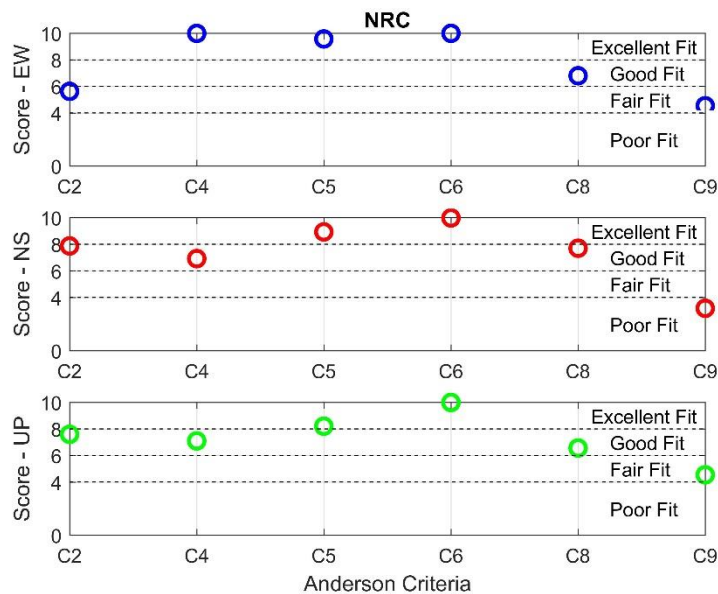


Figure 4.11. Goodness-of-fit (GoF) scores according to Anderson (2004) for NRC station (model S-4) on the three components of motion in the frequency band 0.1-1.5 Hz. C2 = Energy Duration; C4 = Energy Integral; C5 = PGA; C6 = PGV; C8 = Response Spectrum; C9 = Fourier Spectrum.

4.3.3. Generation of ground shaking maps

Starting from the results of 3D numerical simulation, ground shaking maps were generated in terms of both Peak Ground Velocity (PGV, Figure 4.12 to Figure 4.13) and permanent ground displacement (Figure 4.15 to Figure 4.17). As shown in Figure 4.12, the agreement between simulated (Model S-4) and observed peak ground velocity values is satisfactory on the three components of motion not only in terms of spatial distribution, but also in terms of their magnitudes.

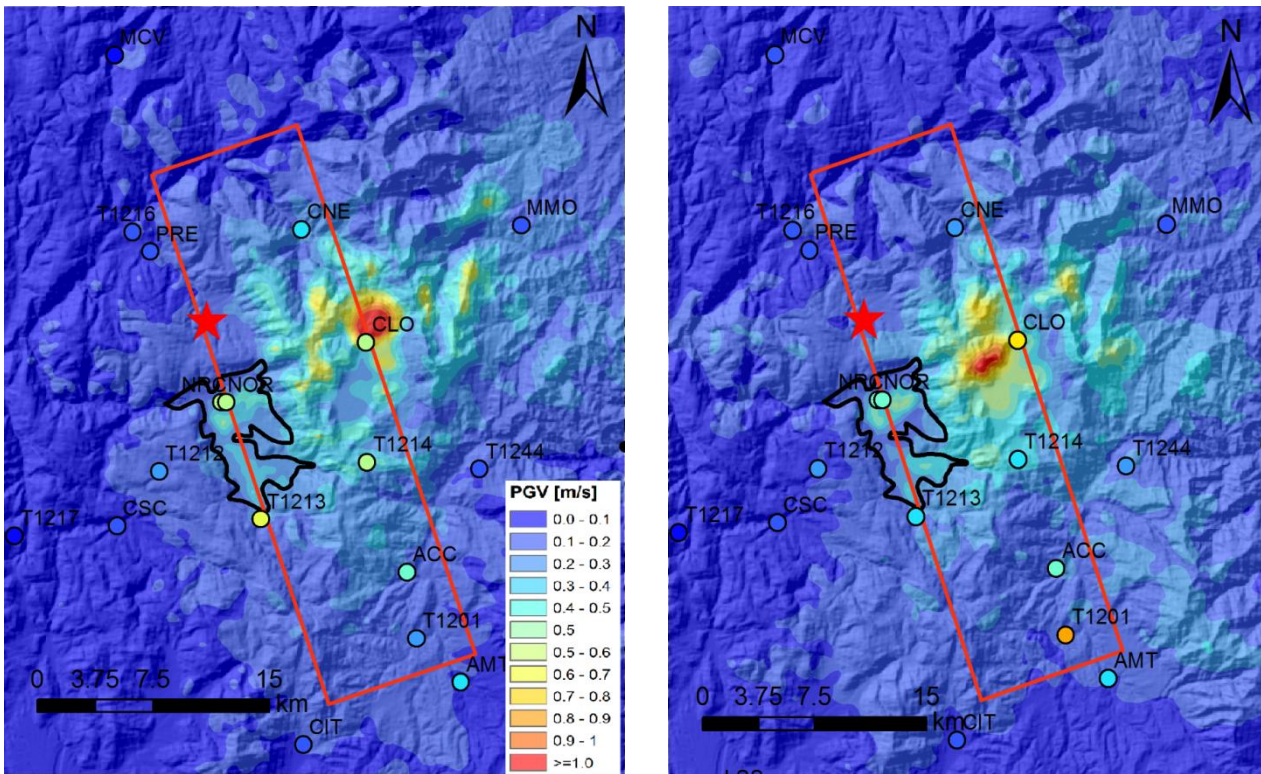


Figure 4.12. Peak ground velocity maps (in m/s) from SPEED simulation (Model S-4) for EW (left) and NS (right) component. Coloured circles represents the corresponding values obtained from recordings. Same colour scale is used to represent the results of the simulation and recordings.

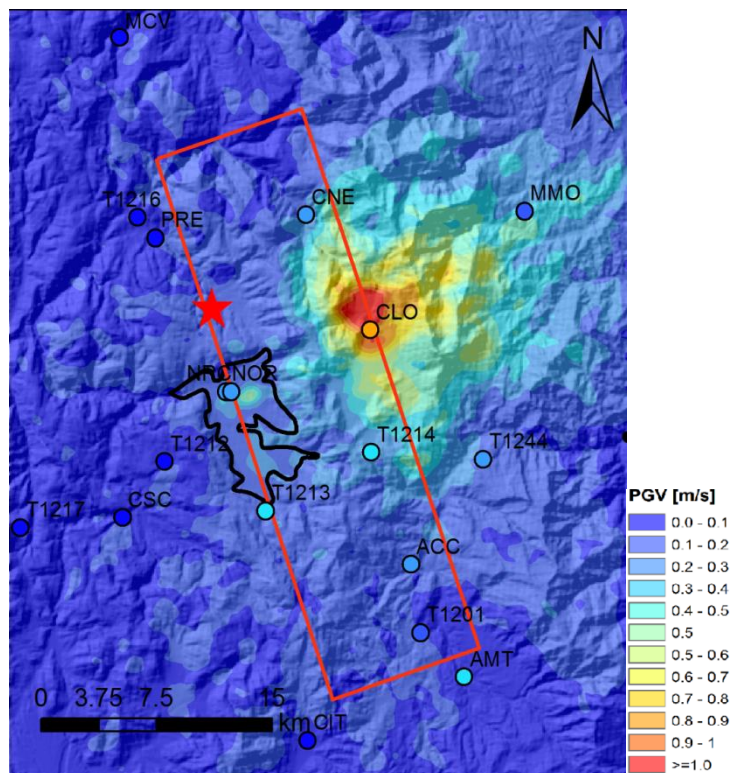


Figure 4.13. Same as in Figure 4.12 but for vertical component.

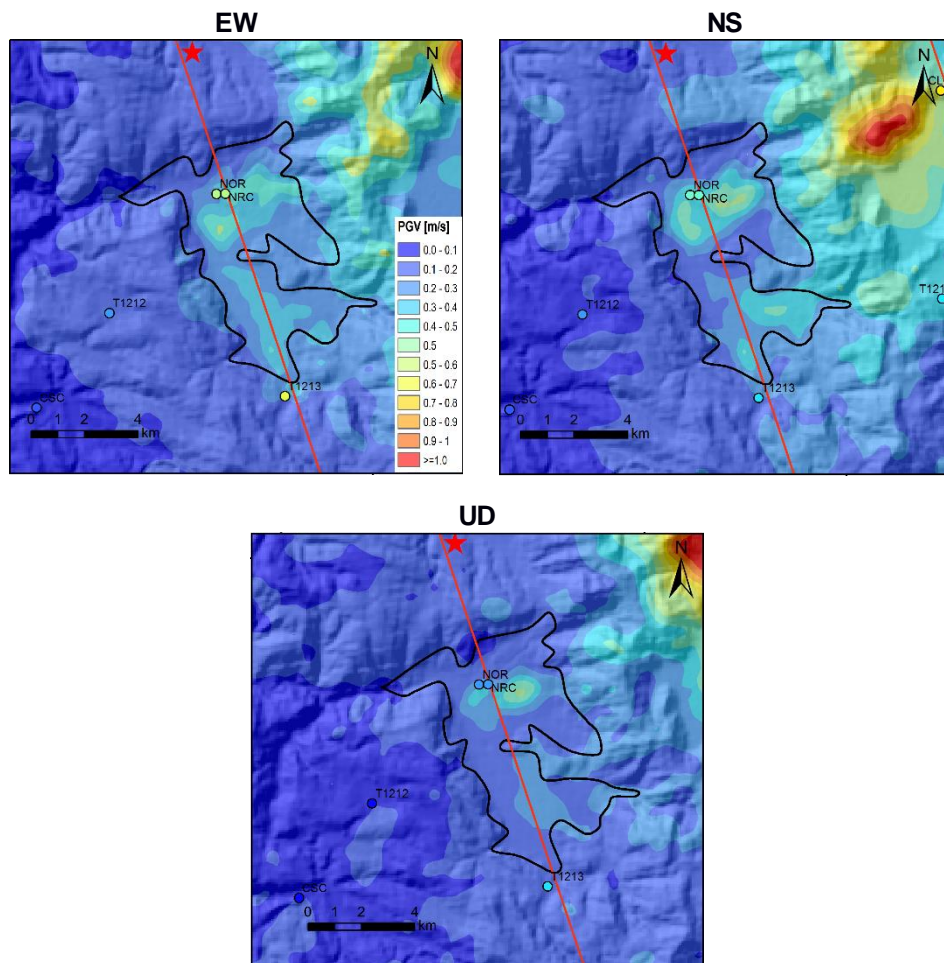


Figure 4.14. Close-up view of the PGV maps of Figure 4.12 and Figure 4.13. Same as in Figure 4.12 but for vertical component.

Distributions of the permanent ground displacements of the 3D model are compared with independent SAR measurements (Atzori, 2017). Those comparisons are provided in Figure 4.15 to Figure 4.17.

By considering EW and Vertical components, it could be concluded that SPEED models reliably capture the measured quantities of residual displacements. Yet, there is an inconsistency present along NS direction which is believed to be stemming from a complex rupture mechanism that could not be explained with a single source with rectangular geometry (Cheloni et al., 2017).

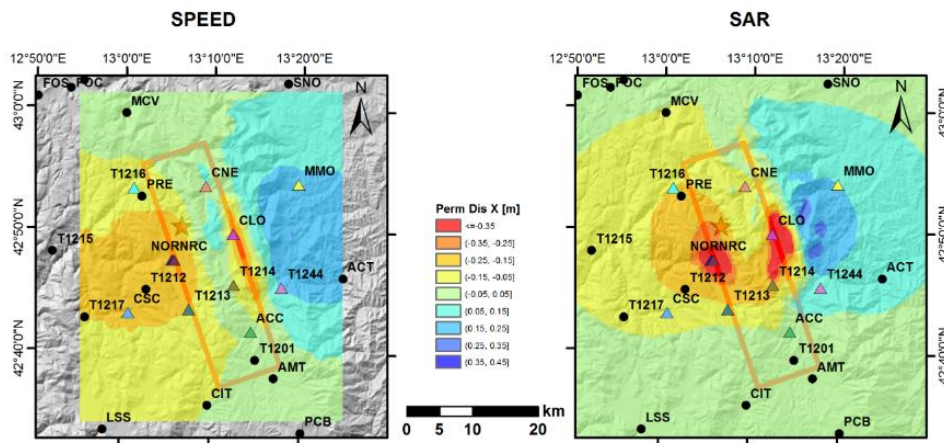


Figure 4.15. Comparisons of residual displacements with SAR measurements (East-West component)

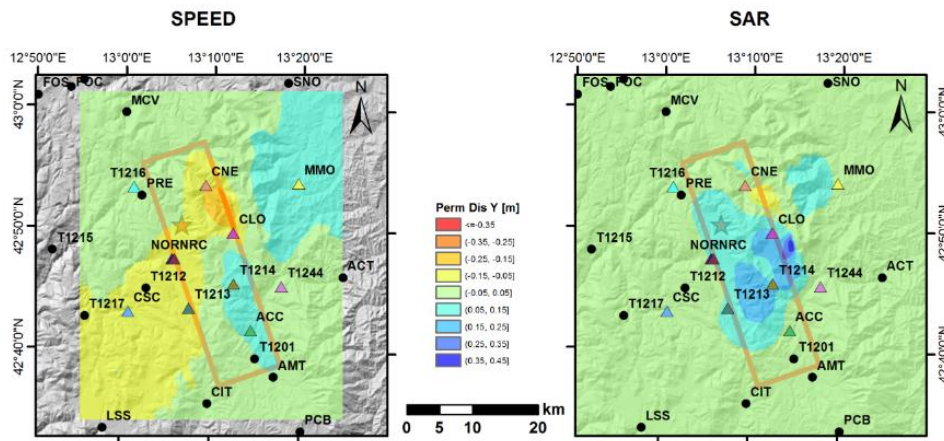


Figure 4.16. Comparisons of residual displacements with SAR measurements (North-South component)

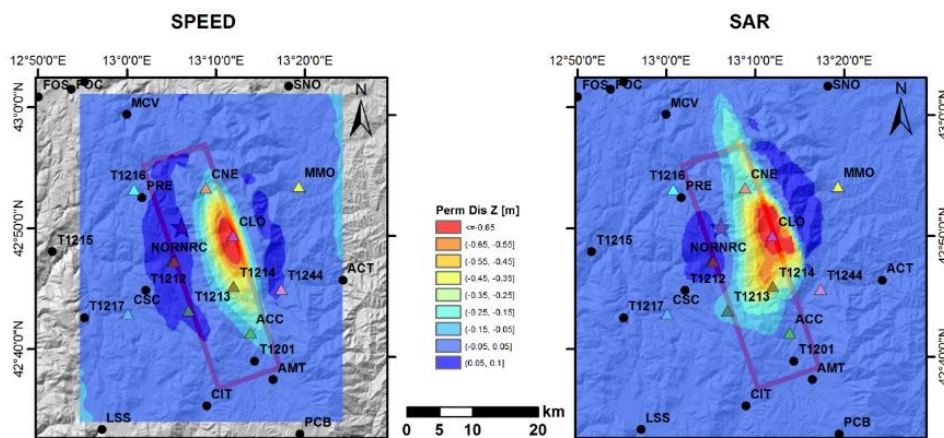


Figure 4.17. Comparisons of residual displacements with SAR measurements (Vertical component)

4.3.4. Broadband ground motions

Starting from the results of 3D simulations (model S-4), reliable up to 1.5 Hz, broadband ground motions have been generated for the Norcia area using the ANN2BB procedure presented in Chapter 2. It is underlined that, with respect to the procedure illustrated previously, broadband response spectra are obtained herein by averaging the results of 20 different ANNs, trained on the same SIMBAD database. Checks have pointed out that the training multiple neural networks and, then, averaging their outputs improve generalization and increase significantly the robustness of results.

In Figure 4.18 to Figure 4.19, broadband (ANN2BB) peak ground acceleration (PGA) are provided and compared with the values registered at corresponding strong ground motion recorders. It could be commented that the spatial distributions of the PGA magnitudes are better approximated along the horizontal components (i.e. EW and NS) than the vertical one (V), because performance of ANN is generally lower for vertical motions (see Chapter 2). When the focus is given to the PGA maps generated for EW and NS directions, it could be observed that the motion within the basin is consistently overestimated, most likely because of imposed linear constitutive relation of the basin sediments. Such overestimation is expected to decrease when material nonlinearity will be accounted for in future works.

Furthermore, to evaluate the spatial correlation structure of the simulated PGA field, we computed the semivariograms for the synthetic PGA values (geometric mean of horizontal components), using the procedure outlined in Section 3. The results, reported in Figure 4.20, indicate that the value of range resulting from the best-fitting exponential model is around 27 km. This value is larger than the one found by Esposito and Iervolino (2012) on the entire Italian dataset ITACA, owing to the simplified velocity model assumed outside the Norcia basin. However, it is interesting to note that the range value obtained from the 3D model shows a general consistency with the values found by Jayaram and Baker (2009) for individual earthquakes in a similar seismo-tectonic context.

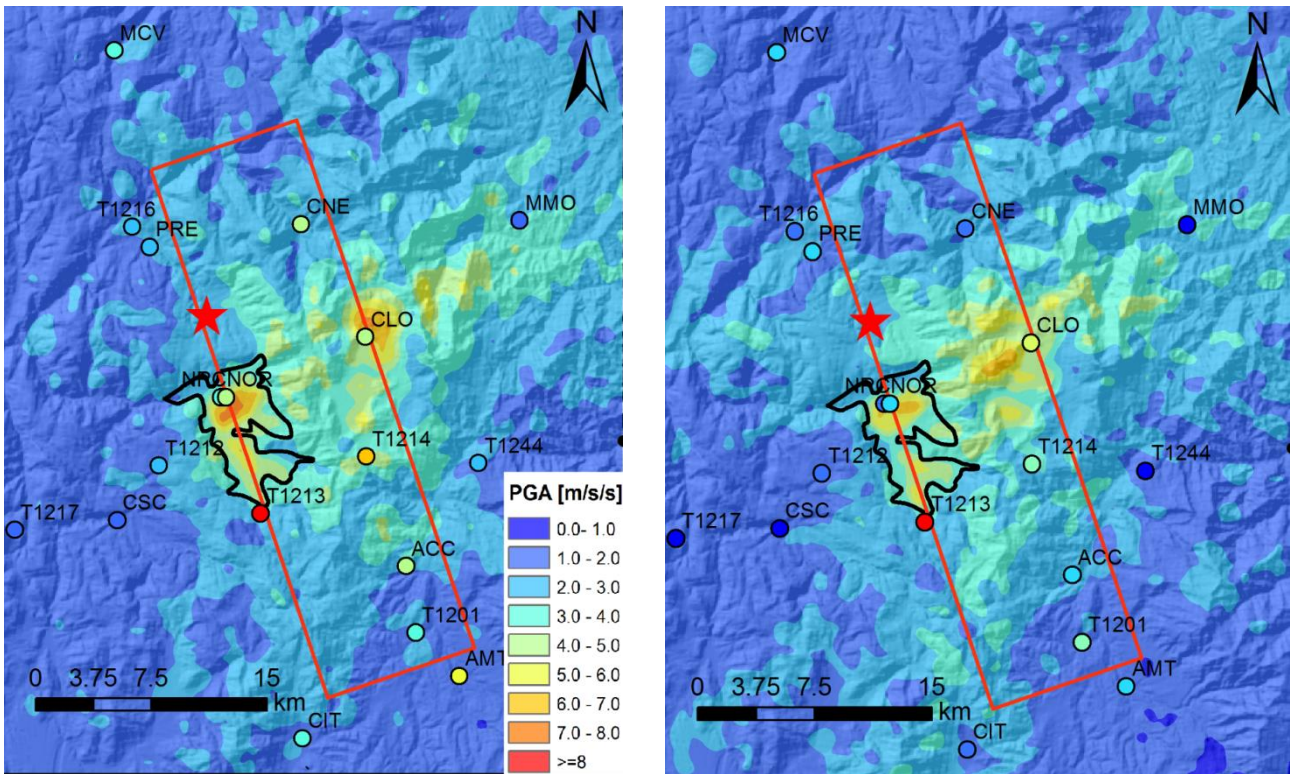


Figure 4.18. Broadband peak ground acceleration (PGA) maps (in m/s^2) through ANN2BB procedure for EW component. Coloured circles represents the corresponding values obtained from recordings. Same colour scale is used to represent the results of the simulation and recordings.

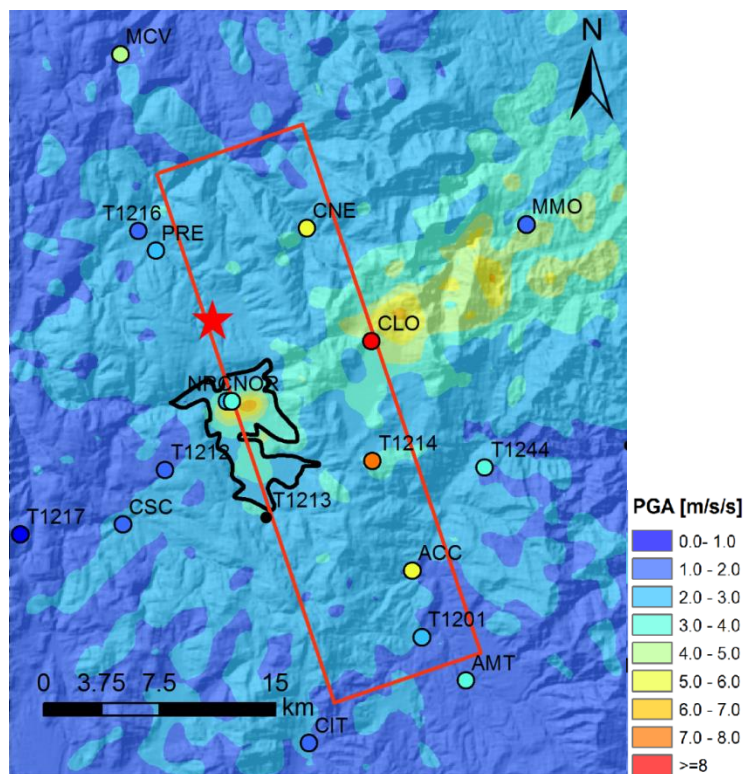


Figure 4.19. Same as in Figure 4.12 but for vertical component.

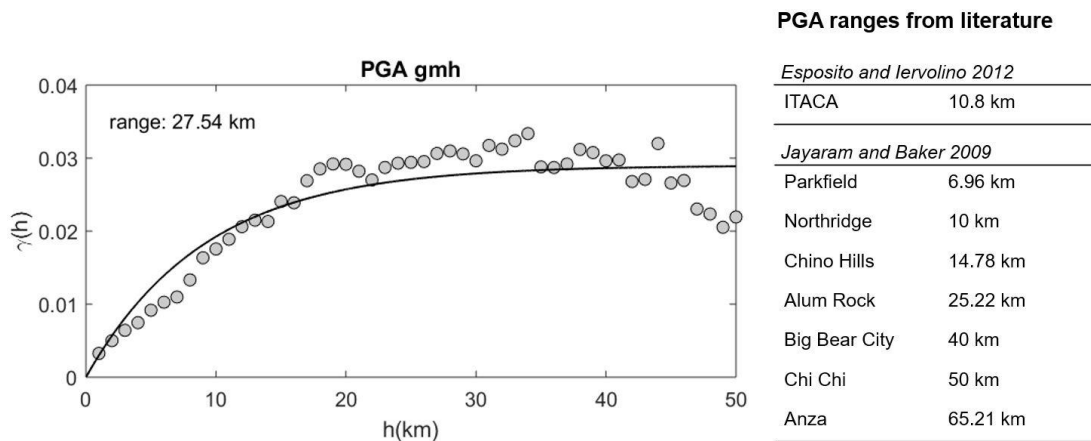


Figure 4.20 Semi-variograms estimated from synthetic PGA values (geometric mean of horizontal components). The *range* associated with the best-fitting exponential model (dashed lines), is shown and compared with literature values.

Figure 4.21 shows the comparison between recordings and ANN2BB synthetics at two stations, namely NRC (a) and CNE (b), for EW and NS component, respectively, in terms of ground motion time histories (top) and spectral features (response and Fourier spectra, bottom). Results indicate a good agreement between observations and recordings also in the high frequency range and show realistic features of synthetics both in time and frequency domain.

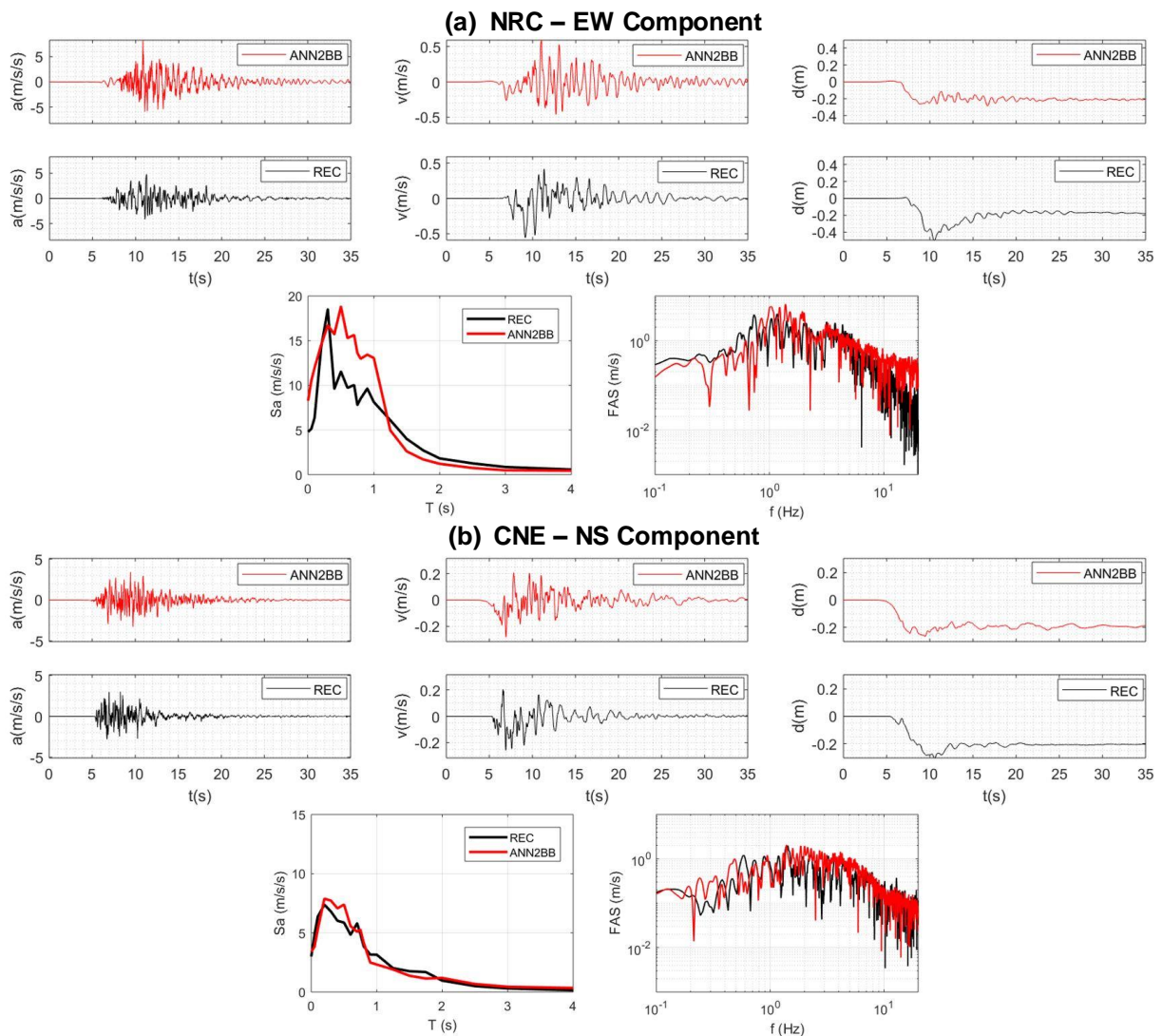


Figure 4.21. Comparison between recordings (black) and ANN2BB synthetics (red) at (a) NRC, EW component and (b) CNE, NS component: acceleration, velocity and displacement time histories (top, from left to right); acceleration response spectra (bottom, left) and Fourier Amplitude Spectra (bottom, right).

References

- Anderson, J.G. (2004). Quantitative measure of the goodness-of-fit of synthetic seismograms, in Proceedings of the 13th World Conference on Earthquake Engineering, 2004 August 16, Vancouver, British Columbia, Canada, Paper No. 243.
- Andrews, D. (1976). Rupture propagation with finite stress in antiplane strain, *J. Geophys. Res.*, 81, 3575–3582.
- Angeletti A, et al. (2018). Personal communications: geophysical in-situ test data.
- Aringoli D, Cavitolo P, Farabollini et al. (2014). Morphotectonic characterization of the quaternary intermontane basins of the Umbria-Marche Apennines (Italy), *Rend. Fis. Acc. Lincei*, 25(Supp 2): 111-128, doi: 10.1007/s12210-014-0330-0.
- Atzori S. (2018). *Personal communications: In-SAR data for the 2016 October 30th earthquake.*
- Benjmama, M., N. Glinsky-Olivier, V. Cruz-Atienza, and J. Virieux (2009), 3-D dynamic rupture simulations by a finite volume method, *Geophys. J. Int.*, 178, 541560
- Bindi D, Luzi L, Parolai S, Di Giacomo D, Monachesi G (2011a). Site effects observed in alluvial basins: the case of Norcia (Central Italy), *Bulletin of Earthquake Engineering*, 9: 1941-59, doi: 10.1007/s10518-011-9273-3.
- Böhm G, Luzi L, Galadini F (2011). Tomographic depth velocity model below the plain of Norcia (Italy) for site effect studies. *Bollettino di Geofisica Teorica ed Applicata*, 52(2), doi: 10.4430/bgta0002.
- Cauzzi C, Faccioli E, Vanini M, Bianchini A (2015) Updated predictive equations for broadband (0.01 - 10 s) horizontal response spectra and peak ground motions, based on a global dataset of digital acceleration records. *Bulletin of Earthquake Engineering* 13(6): 1587-1612.
- Chaljub E, Moczo P, Tsuno S, Bard PY, Kristek J, Kaser M, Stupazzini M, Kristekova M (2010) Quantitative comparison of four numerical predictions of 3D ground motion in the Grenoble valley, France. *Bull Seismol Soc Am* 100:1427–1455
- Cheloni D, De Novellis V, Albano M et al. (2017) Geodetic model of the 2016 Central Italy earthquake sequence inferred from InSAR and GPS data. *Geophysical Research Letters*, 44, 6778-6787.
- Chiaraluce, L., Di Stefano, R., Tinti, E., Scognamiglio L., Michele, M., Casarotti, E., Cattaneo, M., De Gori, P., Chiarabba, C., Monachesi, G. et al. (2017). The 2016 central Italy seismic sequence: A first look at the mainshocks, aftershocks, and source models, *Seismol. Res. Lett.*, 88(3), doi: 10.1785/0220160221.
- A. K. Chopra, 1995. *Dynamics of Structures: Theory and Applications to Earthquake Engineering.* Prentice-Hall.
- Dalguer, L., and S. Day (2007), Staggered-grid split-node method for spontaneous rupture simulation, *J. Geophys. Res.*, 112, B02,302.
- Day SM, Bradley CR. Memory-efficient simulation of anelastic wave propagation. *Bulletin of the Seismological Society of America* 2001; 91(3):520–531.
- Day, S., L. Dalguer, N. Lapusta, and Y. Liu (2005), Comparison of finite difference and boundary integral solutions to three-dimensional spontaneous rupture, *J. Geophys. Res.*, 110, B12,307
- Dieterich, J. H. (1979), Modeling of rock friction 1. experimental results and constitutive equations, *J. Geophys. Res.*, 84(B5)
- Emmerich, H., M. Korn 1987. Incorporation of attenuation into time-domain computations of seismic
- Paolucci et al.* –Progress report on 3D physics-based numerical approaches for earthquake ground motion prediction- SIGMA2-2018-D3-015

- wave fields. *Geophysics* 52, 1252–1264.
- Esposito S., Iervolino I. (2012). Spatial Correlation of Spectral Acceleration in European Data, *Bull. Seismol. Soc. Am.* 102, no. 6, 2781–2788
- Evangelista L., del Gaudio S., Smerzini C., d’Onofrio A., Festa G., Iervolino I., Landolfi L., Paolucci R., Santo A., and Silvestri F.. Physics-based seismic input for engineering applications: a case study in the Aterno River valley, Central Italy. *Bulletin of Earthquake Engineering*, 15(7):2645–2671, 2017
- Galvez, P., J.-P. Ampuero, L. Dalguer, and T. Nissen-Meyer (2011), Dynamic rupture modelling of the 2011 M9 Tohoku earthquake with unstructured 3D spectral element method, *Eos Trans. AGU*, 1(1), Fall Meet. Suppl., Abstract S24.
- Geubelle, P., and J. Rice (1995), A spectral method for three-dimensional elastodynamic fracture problems, *J. Mech. Phys. Solids*, 43, 1791–1824.
- Harris, R., et al. (2004), The source physics of large earthquakes: Validating spontaneous rupture methods, *Eos Trans. AGU*, 85(47), Fall Meet. Suppl., Abstract S12A–05.
- Herrmann, R. B., Malagnini, L., & Munafò, I. (2011). Regional moment tensors of the 2009 L’Aquila earthquake sequence. *Bulletin of the Seismological Society of America*, 101(3): 975-993.
- Hisada Y, Bielak J (2003). A Theoretical Method for Computing Near-Fault ground Motions in Layered Half-Spaces Considering Static Offset Due to Surface Faulting, with a Physical Interpretation of Fling Step and Rupture Directivity, *Bulletin of the Seismological Society of America*, 93(3), 1154-1168.
- Jayaram N., Baker J.W. (2009). Correlation model for spatially distributed ground motion intensities, *Earthq. Eng. Struct. Dynam.* 38, no. 15, 1687–1708.
- Kaneko, Y., N. Lapusta, and J.-P. Ampuero (2008), Spectral element modeling of spontaneous earthquake rupture on rate and state faults: Effect of velocity-strengthening friction at shallow depths, *J. Geophys. Res.*, 113, B09,317.
- Kosloff R, Kosloff D (1986) Absorbing boundaries for wave propagation problems. *J Comput Phys* 63(2):363–376
- Kramer SL (1996) *Geotechnical earthquake engineering*. Prentice-Hall, Upper Saddle River
- Liu C, Zheng Y, Xie, Z, Xiong, X (2017). Rupture features of the 2016 Mw 6.2 Norcia earthquake and its possible relationship with strong seismic hazards, *Geophys. Res. Lett.* 44, 1320–1328, doi:10.1002/2016GL071958.
- Mase, C., and L. Smith (1985), Pore-fluid pressures and frictional heating on a fault surface, *Pure and Applied Geophysics*, 122, 583–607.
- Mazzieri I, Stupazzini M, Guidotti R, Smerzini C (2013) SPEED: SPectral Elements in Elastodynamics with Discontinuous Galerkin: a non-conforming approach for 3D multi-scale problems. *Int J Numer Meth Eng* 95(12):991–1010
- Moczo, P., J. Kristek, M. Galis, P. Pazak, and M. Balazovjeh (2007), The finite-difference and finite-element modeling of seismic wave propagation and earthquake motion, *Acta physica slovacica*, 57(2), 177–406.
- Motti (2017). Personal communications for the document: “Progetto cartografie geologiche e geotematiche delle aree terremotate finalizzate all’individuazione della pericolosità sismica locale-Sezioni 337010 “Serravalle” 337020 “Norcia” 325130 “Todiano” 325140 “Ancarano”, Scala:1:10000”

- NIST - National Institute of Standards and Technology (2011). Selecting and scaling earthquake ground motions for performing response history analyses, Technical Report NIST GCR 11-917-15, prepared for the Engineering Laboratory of the National Institute of Standards and Technology (NIST) under the National Earthquake Hazards Reduction Program (NEHRP) Earthquake Structural and Engineering Research Contract SB134107CQ0019, Task Order 69220, November 2011.
- Paolucci R., Mazzieri I., Smerzini C. (2015). Anatomy of strong ground motion: near-source records and 3D physics-based numerical simulations of the Mw 6.0 May 29 2012 Po Plain earthquake, Italy, *Geophys. J. Int.* 203, 2001–2020.
- Pelties, C., M. Käser, V. Hermann, and C. E. Castro (2010), Regular versus irregular meshing for complicated models and their effect on synthetic seismograms, *Geophys. J. Int.*, 183(2) 1031–1051
- Pizzi A, Di Domenica A, Gallovič F, Luzi L, Puglia R (2017). Fault segmentation as constraint to the occurrence of the main shocks of the 2016 Central Italy seismic sequence. *Tectonics*, 36(11), 2370-2387.
- Porreca M, Vassallo M (2018). Personal communications: geophysical in-situ test data and expert opinion.
- Ruina, A. L. (1983), Slip instability and state variable friction laws, *J. Geophys. Res.*, 88, 10,359–10,370.
- Sabetta F., Pugliese A. (1996). Estimation of Response Spectra and Simulation of Nonstationary Earthquake Ground Motions, *Bull. Seismol. Soc. Am.* 86, no. 2, 337–352.
- Smerzini C., Villani M. (2012). Broadband Numerical Simulations in Complex Near-Field Geological Configurations: The Case of the 2009 Mw 6.3 L'Aquila Earthquake, *Bull. Seismol. Soc. Am.* 102, no. 6, 2436–2451.
- Smerzini C., Galasso C., Iervolino I., Paolucci R. (2014). Ground motion record selection based on broadband spectral compatibility, *Earthq. Spectra* 30, no. 4, 1427–1448.
- Stupazzini M., Paolucci R., Igel H. (2009). Near-fault earthquake ground-motion simulation in Grenoble Valley by high-performance spectral element code. *Bull Seismol Soc Am* 99(1):286–301, doi: 10.1785/0120080274
- Tada, T., and R. Madariaga (2001), Dynamic modelling of the flat 2-D crack by a semi-analytic BIEM scheme, *International Journal for Numerical Methods in Engineering*, 50(1), 227–251
- Venanti LD (2018). Personal communications: geotechnical laboratory test data and expert opinion.

	Research and Development Program on Seismic Ground Motion	Ref : SIGMA2-2018-D3-015
		Page 39/41

APPENDIX 1

This Appendix reports the mathematical and numerical formulation of the SPEED dynamic rupture model presented in Chapter 1.

	Research and Development Program on Seismic Ground Motion	Ref : SIGMA2-2018-D3-015
		Page 40/41

APPENDIX 2

This appendix reports the paper entitled “Broad-band ground motions from 3D physics-based numerical simulations using Artificial Neural Networks”, by R. Paolucci, F. Gatti, M. Infantino, C. Smerzini, A.G. Özcebe and M. Stupazzini, published in the Bulletin of Seismological Society of America, 2018, doi: 10.1785/0120170293

	Research and Development Program on Seismic Ground Motion	Ref : SIGMA2-2018-D3-015
		Page 41/41

APPENDIX 3

This appendix reports the paper entitled “Analysis of the spatial correlation of earthquake ground motion from physics-based numerical simulations”, by M. Infantino, R. Paolucci, and C. Smerzini, published in the proceedings of the Workshop BestPSHANI 2 - Best Practices in Physics-based Fault Rupture Models for Seismic Hazard Assessment of Nuclear Installations: issues and challenges towards full Seismic Risk Analysis-, Cadarache-Château, France, 14-16 May 2018.